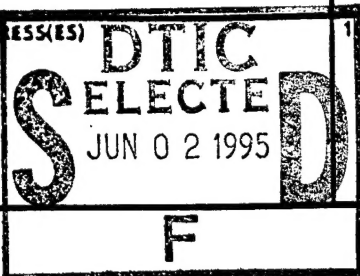


ORIGINAL

REPORT DOCUMENTATION PAGE			Form Approved OMB No. 0704-0188	
<small>Public reporting burden for this collection of information is estimated to average 1 hour per response, including the time for reviewing instructions, searching existing data sources, gathering and maintaining the data needed, and completing and reviewing the collection of information. Send comments regarding this burden estimate or any other aspect of this collection of information, including suggestions for reducing this burden, to Washington Headquarters Services, Directorate for Information Operations and Reports, 1215 Jefferson Davis Highway, Suite 1204, Arlington, VA 22202-4302, and to the Office of Management and Budget, Paperwork Reduction Project (0704-0188), Washington, DC 20503.</small>				
1. AGENCY USE ONLY (Leave blank)	2. REPORT DATE May 1995	3. REPORT TYPE AND DATES COVERED Final Technical Report 4/1/91-3/31/95		
4. TITLE AND SUBTITLE Direct and Large Eddy Simulation of Separated Turbulent Boundary Layers			5. FUNDING NUMBERS N00014-91-J-1877	
6. AUTHOR(S) Professor Parviz Moin				
7. PERFORMING ORGANIZATION NAME(S) AND ADDRESS(ES) Stanford University Mechanical Engineering Thermosciences Division Stanford, CA 94305-3030			8. PERFORMING ORGANIZATION REPORT NUMBER 2-DJA-529	
9. SPONSORING/MONITORING AGENCY NAME(S) AND ADDRESS(ES) Office of Naval Research Dr. James Fein 800 North Quincy Street Arlington, VA 22217-5000			10. SPONSORING/MONITORING AGENCY REPORT NUMBER	
11. SUPPLEMENTARY NOTES				
12a. DISTRIBUTION/AVAILABILITY STATEMENT Approved for public release. Distribution is unlimited.			12b. DISTRIBUTION CODE *Original contains color plates: All DTIC reproductions will be in black and white*	
13. ABSTRACT (Maximum 200 words) Space-time characteristics of pressure fluctuations were analyzed using the databases generated from the direct numerical simulation. In the separated flow, the wall-pressure fluctuations are significantly reduced in the separation zone. However, they are significantly enhanced in the reattachment region. The streamwise and spanwise vorticities are lifted away from the wall in the separation zone and the pressure fluctuations are significantly enhanced in this shear layer. The contours of space-time correlations show that the convection velocities of wall-pressure fluctuations are reduced significantly inside the separation bubble. The reattachment region is characterized by large scale structures which are formed in the shear layer above the separation bubble. Frequency spectra downstream of incipient detachment shows that maximum turbulent shearing stress $-\rho u'v'_{max}$ appears to be the proper scale to normalize wall-pressure fluctuations in the turbulent boundary layers in the presence of large adverse pressure gradient.				
14. SUBJECT TERMS separated turbulent boundary layer, frequency spectra of wall-pressure, space-time correlation of pressure fluctuations			15. NUMBER OF PAGES	
			16. PRICE CODE	
17. SECURITY CLASSIFICATION OF REPORT unclassified	18. SECURITY CLASSIFICATION OF THIS PAGE unclassified	19. SECURITY CLASSIFICATION OF ABSTRACT unclassified	20. LIMITATION OF ABSTRACT	

19950601 024

Final Technical Report for:

**DIRECT AND LARGE EDDY SIMULATION
OF SEPARATED TURBULENT BOUNDARY LAYERS**

Project #N00014-91-J-1877

Submitted by:

Parviz Moin
Stanford University
Mechanical Engineering, Thermosciences Division
Stanford, CA 94305-3030
Phone: (415) 723-9713

Accession For	
NTIS CRA&I	<input checked="" type="checkbox"/>
DTIC TAB	<input type="checkbox"/>
Unannounced	<input type="checkbox"/>
Justification	
By	
Distribution /	
Availability Codes	
Dist	Avail and/or Special
A-1	

Submitted to:

James Fein
Office of Naval Research
Fluid Dynamics Branch
Arlington, VA 22217-5000
Phone: (703) 696-4715

For the Period:

April 1, 1991 through March 31, 1995

FINAL TECHNICAL REPORT

1. Direct & large eddy simulation of separated turbulent boundary layers

Contract number: N00014-91-J-1877

Principal Investigator: Parviz Moin, Stanford University

ONR Program Manager: Dr. James Fein

2. Introduction

Understanding the onset of separation is important because it represents the upper limit of efficiency for many flow devices such as diffusers, airfoils, turbine blades *etc.*. But the structure of the separated region is poorly understood. The prediction methods based on the Reynolds averaged equations have significant shortcomings in the separated flows. Difficulties arise both in the prediction of the inception of separation and in the subsequent flow development. Currently there are only very limited experimental data available in the backflow region. For a steady free-stream separating turbulent boundary layer, reversal of the flow in the boundary layer begins intermittently upstream of the mean detachment point; that is the flow reversal occurs only a fraction of the time. Further downstream, the fraction of time that flow moves downstream progressively decreases. In the traditional view, the entire backflow came from far downstream. But the modern view is that large scale outer coherent structures supply the intermittent backflow and the flow towards the wall.

The behavior of wall-pressure fluctuations in turbulent boundary layers is also of fundamental importance in many practical applications involving flow induced vibration, aircraft cabin noise and hydro-acoustics characteristics of underwater vehicles. Models of flow induced vibration and sound require the frequency/wave-number spectrum of wall pressure-fluctuations as the forcing function input for the structural model. For a comprehensive treatment of the subject see Blake (1986). Accurate measurements are made difficult by sensitivity to the measuring probe or the transducer size, and the wide range of scales of the pressure fluctuations. In general, the complete wall-pressure data needed for turbulence/structure interaction models is lacking. Effects of adverse pressure gradient on the wall pressure fluctuations have been studied experimentally by Simpson *et. al* (1989) and others. Much higher levels of noise and pressure fluctuations are produced by a separated flow as compared to an attached boundary layer. In the separated flows velocity fluctuations are comparable to the mean velocity in the backflow region. Since the Reynolds shear stress and their gradients are largest away from the wall in separated flows, it has been speculated that the largest pressure fluctuations are not at the wall but away from it. Structure of pressure fluctuations away from the wall is likely to be critical to the prediction and our understanding of turbulent boundary layer acoustics.

In many separated flows (e.g., flow over airfoils), both the surface curvature and adverse pressure gradients influence the detachment of turbulent boundary layer. However, to

isolate the effects of the adverse pressure gradient, it would be instructive to consider a flat plate surface with an imposed pressure gradient. Such studies were conducted by Perry & Fairlie (1975), Cutler & Johnston (1984) and Patrick (1987). Although a number of other investigators have conducted *closed* separation bubble studies, most of their test geometries involved rapid surface curvature or sharp edges producing fixed separation points. A recent review of the experimental studies of turbulent boundary layer separation is given by Simpson (1989).

3. Objective

The objective of this research is to compute and study the space-time characteristics of pressure fluctuations in turbulent boundary layers under **adverse pressure** gradient and in **separated** turbulent boundary layers. Numerical simulations are ideal for this purpose because pressure fluctuations within the flow can not be measured experimentally. At present, the complete three dimensional frequency/wave-number spectrum can only be obtained from direct numerical simulation.

4. Technical Approach

Direct numerical simulation technique is used to provide a comprehensive data set for flow analysis. We have developed a code for the present purpose and made extensive comparisons with the experimental data of zero pressure gradient (ZPG) turbulent boundary layers and turbulent boundary layers with adverse pressure gradient (Watmuff (1989)). The code solves the three dimensional, time-dependent incompressible Navier-Stokes equations on a staggered grid. All spatial derivatives are approximated with second-order central differences. Governing equations are time-advanced with a low-storage three-substep third order Runge-Kutta scheme which has an explicit treatment for the convection terms and implicit treatment for the viscous terms. The three-substep Runge-Kutta scheme is combined with the fractional step procedure.

The key technical issues for direct numerical simulations of adverse pressure gradient and separated flows are:

- Proper boundary conditions in the free-stream that can lead to separation and the subsequent reattachment.
- Proper inflow boundary conditions that result in physically realistic turbulence in a relatively small portion of the computational domain.

Our work on the free-stream boundary conditions in the adverse pressure gradient turbulent boundary layer flow revealed that when both the streamwise velocity, u , and the normal velocity, v , obtained from the potential flow solution, are simultaneously prescribed the result is numerical oscillations away from the wall. Since most experiments measure and report the streamwise velocity at the boundary layer edge, we developed a technique that given the edge streamwise velocity, computes the corresponding normal velocity at the same locations. This normal velocity and the normal derivative of the streamwise velocity condition (from the zero-vorticity condition) are then prescribed as the well-posed

boundary conditions for Navier-Stokes computations.

We have made a major advance on a key item for direct and large eddy simulation of complex flows: prescription of turbulent inflow conditions. A good strategy for prescription of the unsteady, stochastic inflow conditions would lead to a significant reduction in the computational cost. Our earlier approach was to prescribe velocity fluctuations superimposed on a mean profile with a specified power spectrum and random phase. This inflow turbulence lacked any structure and required significant spatial development to become physically realistic. Our new technique consists of a sequential feeding at the inflow plane of a frozen DNS field with some randomization of amplitude factors. Simulations using these boundary conditions show remarkably fast adjustment.

In the simulation of adverse pressure gradient boundary layer, the free-stream boundary condition (blowing-suction velocity distribution) was iteratively adjusted to match the wall-pressure distribution and the Reynolds number of Watmuff (1989)'s experiment. In the separated turbulent boundary layer flow, a suction-blowing velocity profile along a virtual top wall is used to create an adverse-to-favorable pressure gradient that produces a closed separation bubble (thickness of the bubble is approximately twice the inlet boundary thickness). The Reynolds number based on inlet displacement thickness is 500. The simulation of adverse pressure gradient flow used approximately 18 megawords of memory and required 31 CPU seconds per time step on the Cray-C90 with $769 \times 65 \times 257$ grid points. In the separated flow, the required core memory is 9 megawords and CPU time per time step is 31 seconds with $513 \times 193 \times 129$ grids.

5. Technical Accomplishments

(5.1) Zero-pressure gradient turbulent boundary layer

Direct numerical simulation of spatially developing turbulent boundary layer subject to zero pressure gradient has been also performed to validate our code for the present study. In the zero pressure gradient boundary layer, frequency spectra, two-point correlations and convection velocities of wall pressure fluctuations are in very good agreement with experimental data and the results of numerical simulation of channel flow. The comparisons of the computed power spectrum with the experimental data are provided in figures 1-2. In figure 1, normalization with outer scales is used. All the experimental data and simulation results collapse at low frequencies. When normalized with the inner variables, the data from the simulation and the experiments appear to collapse at high frequencies (Figure 2). The effect of Reynolds number can be established from figures 1-2. With increasing Reynolds number, power increases in the high-frequency region with outer scale. With increasing Reynolds number, power increases in the low frequency region with inner scaling.

"Convection" velocity can be defined in a number of ways and can be expressed as function of the streamwise separation r_x , the temporal separation r_t . A commonly used definition is the ratio r_x/r_t , which makes the space-time correlation of wall-pressure fluctuations, $R(r_x, r_t)$, a maximum. Convection velocity of wall-pressure fluctuations obtained using this definition shows agreement with the experimental data (Figure 2). Large-scale

structures corresponding to the large separations in space or time have a convection velocity of about $0.8 U_0$. Small-scale motions have a smaller velocity, 0.65 to $0.7 U_0$.

(5.2) Favorable-adverse-pressure gradient turbulent boundary layer

In the favorable and adverse pressure gradient flow, C_p distribution of Watmuff(1989)'s experiment was matched. Wall-pressure coefficient and skin friction coefficient are compared over the entire domain in figure 3. The agreement is very good. The maximum difference is about 4 %. Other global quantities such as displacement and momentum thicknesses are also in good agreement with the experimental data. Root-mean square velocity profiles at two streamwise locations in the adverse pressure gradient region are shown in figure 4. The agreement is best for u_{rms} , which is usually measured more accurately because it is measured with a normal hot wire instead of an X-wire. In figure 5, the frequency spectra of wall-pressure fluctuations normalized with the outer variables are shown at several streamwise locations. $X=0.5$ is in the favorable pressure gradient region and the remaining points are in the adverse pressure gradient regions. The results collapse at low frequencies. When the spectra are normalized by p_{rms} , results appear to collapse at high frequencies(Figure 6). Notice that in the zero-pressure gradient boundary layer results collapse at high frequencies when normalized by $\nu\tau_w^2/u_\tau^2$. Since the wall shear stress τ_w or friction velocity u_τ decreases significantly and even can be negative in the adverse pressure gradient or separated flows, they are not expected to be good scalings for the pressure. The contours of constant two-point spatial correlation of wall pressure fluctuations at two streamwise locations are shown in figure 7. The contour shapes at small separations are circular, but at larger separations are oval shaped, indicating that the large structures contributing to wall-pressure fluctuations are more elongated in the spanwise direction than in the streamwise direction. Note that in the vicinity of the wall, velocity correlation patterns are significantly elongated in the flow direction. The present study shows that the contours of two-point correlation of pressure fluctuations are more elongated in the spanwise direction in the adverse pressure gradient boundary layer as compared to the zero or favorable pressure gradient boundary layers. The convection velocities of wall-pressure fluctuations as a function of spatial and temporal separations are lower in the adverse pressure gradient case(Figure 8).

(5.3) Separated turbulent boundary layer

In the separated flow, as the turbulent boundary layer undergoes an adverse pressure gradient, the flow near the wall decelerates until some backflow first occurs at incipient detachment. A spanwise line of detachment does not move up and downstream as a unit. Small three-dimensional elements of flow move upstream for a distance and are later carried downstream. These reversed flows occur in regions of low kinetic energy and are caused by forces arising from the large-scale structures and adverse pressure gradient. These large eddies grow rapidly in all directions and agglomerate with one another to decrease the average frequency of passage as detachment is approached. Downstream of detachment, high turbulence levels exist in the backflow, with u and v -fluctuations of the same order as $|U|$. The fraction of time with forward flow never reaches zero, indicating that there is no location with backflow all of the time. Figure 9 shows streamline, instantaneous spanwise

vorticities and wall-shear stress distribution in the separated turbulent boundary layer. The thickness of the bubble is approximately twice the inlet boundary layer thickness and the length of the bubble is about 11 inlet boundary layer thicknesses. Instantaneous spanwise vorticities show that they are lifted and then turning around the separation bubble. It is expected that the flow in this shear layer is qualitatively similar to plane mixing layer. In this region, negligible turbulence-energy production occurs in the backflow. Normal stress turbulence-energy production in the outer region supplies turbulence energy to the backflow by turbulence diffusion where it is dissipated. Contours of wall-shear stress shows that the streaky structures disappear in the separated zone and reappear in the detachment region.

Root-mean square pressure fluctuations as a function of wall-normal distance is shown in figure 10. Far upstream of separation bubble, the location of maximum pressure fluctuations occurs very near the wall. Inside the separation bubble, the location of maximum fluctuation is far away from the wall and the pressure fluctuations are significantly enhanced. After the reattachment, the flow starts to redevelop and the location of maximum fluctuation moves towards the wall. Figure 11 shows contour plots of instantaneous pressure fluctuations in the (x,z) -plane at two different wall-normal locations. The wall-pressure fluctuations are significantly reduced in the separation zone. However, they are significantly enhanced in the reattachment region. This enhancement appears to be influenced by wide variations of the velocity of the fluid impinging on the wall and also by wandering of the reattachment location. Unsteady motion in this region may be a combination of the unsteadiness caused by passage of large-scale structures and by unsteadiness associated with the location of the reattachment point fluctuating upstream and downstream. Away from the wall (at $y = 13$), pressure fluctuations are significantly increased above the separation bubble. This increase is apparently due to the rapid movement of the pressure-fluctuation-producing motions away from the wall as the streamwise and spanwise vorticities are lifted away from the wall in the separation zone (Figure 9).

From the perspective of using pressure-fluctuation data to calculate far-field noise due to dipoles, one should probably locate the effective pressure-fluctuation sources along or near the locus of maximum pressure fluctuations or maximum shear-stress position. In figure 12, contour plots of two-point correlation of wall-pressure fluctuations as a function of streamwise and spanwise spatial separations are shown. Far upstream of separation, the shape of contours is similar to those of adverse pressure gradient flow (Figure 7). Inside the bubble, the structures which produce pressure fluctuations become very large compared to those of upstream and are elongated in the spanwise direction. This implies the presence of large 2-D roller-type structure in this region. Downstream of separation, the flow begins to recover and the shape of contours slowly changes back to those of attached boundary layer. Contours of space-time correlations (figure 13) show that the convection velocities of wall-pressure fluctuations decrease as the pressure gradient increases and they are significantly reduced inside the separation bubble. Downstream of the beginning of intermittent backflow, the direction of instantaneous wave oscillating, thus, the long-time-averaged wave speed is significantly lower than that of upstream. The reattachment region is characterized by large scale structures which are formed in the shear layer above the separation

bubble. Figure 14 shows wall-pressure fluctuation spectra $\Phi(\omega)$ for the adverse pressure gradient region upstream of incipient detachment where there is no intermittent backflow near the wall.

It has been argued that the contribution of eddies in the logarithmic region to the wall pressure leads to a -1 slope in the power spectrum (Blake (1986)). Since the Reynolds number considered in the present study is very low, logarithmic layer is not well defined and the contribution to the wall pressure from this layer is negligible. So, the $\Phi(\omega) \sim \omega^{-1}$ region is not expected to be seen in figure 14. At high frequencies, the spectra decay a bit faster than ω^{-3} which is observed experimentally in the strong adverse pressure gradient region. This might be partly due to the low Reynolds effect and partly due to the second order finite difference spatial discretization which was used in the present study. At low frequencies, the spectra level off slightly and this behavior can be seen in the results of adverse pressure gradient flow (Figure 5) and some experimental data. Figure 15 shows the wall-pressure spectra downstream of incipient detachment in two different non-dimensional coordinates. In figure 15-(a), $\Phi(\omega)$ is normalized by local free-stream dynamic pressure q_∞ . Figure 15-(b) shows that normalization on maximum Reynolds shear stress τ_M produces a much tighter correlation indicating that the free-stream dynamic pressure has less direct influence on the pressure spectra than the local streamwise maximum shearing stress. At high frequencies, spectra decay a little bit faster than ω^{-3} for the same reason as in the results of upstream. In the low frequency region, the spectra level off slightly and this behavior is also observed in the results of Simpson (1987).

Figure 16 shows the root-mean square wall-pressure fluctuations normalized on the reference inlet dynamic pressure q_{ref} and the local maximum Reynolds shear stress τ_M . As mentioned earlier, wall-pressure fluctuations are significantly reduced in the separated zone and enhanced in the reattachment region. The comparison shows less variation of wall-pressure fluctuations when normalized on τ_M than normalized by inlet dynamic pressure. From the figures 15-16, maximum turbulent shearing stress $-\rho \overline{u'v'}_{max}$ appears to be the proper scale to normalize pressure fluctuations in the turbulent boundary layers in the presence of large adverse pressure gradient.

6. Significance

We have made the first direct numerical simulations of spatially developing turbulent boundary layer subject to adverse pressure gradient and separated turbulent boundary layer driven by pressure gradient. The simulations have provided a comprehensive database on the pressure fluctuations within the flow. Several pressure related statistics such as frequency spectra and temporal and spatial correlations have been extracted from the data and documented. The databases generated from these computations are expected to be valuable for Reynolds-averaged turbulence modeling efforts as well as for analyzing the characteristics of turbulent boundary layer acoustics in the presence of flow separation.

7. References

Blake, W. K., *Mechanics of flow-induced sound and vibration* (Academic, London, 1986)

Cutler, A. D. & Johnston, J. P., Adverse pressure gradient and separating turbulent boundary layer flows : The effect of disequilibrium in initial conditions, Rept. MD-46, Thermosciences Div., Mech. Eng. Dept., Stanford University, 1984

Patrick, W. P., Flow field measurements in a separated and reattached flat plate turbulent boundary layer, NASA Contractor Report 4052, 1987

Perry, A. E. & Fairlie, B. D., "A study of turbulent boundary-layer separation and reattachment," *Journal of Fluid Mechanics*, vol. 69, 1975

Simpson, R. L., Turbulent boundary layer separation, *Ann. Rev. Fluid Mech*, vol. 21, 1989

Simpson, R. L., Ghodbane, M. & McGrath, B. E., "Surface pressure fluctuations in a separating turbulent boundary layer," *Journal of Fluid Mechanics*, vol. 177, 1987

Watmuff, J. H., An experimental investigation of a low Reynolds number turbulent boundary layer subject to an adverse pressure gradient, *Ann. Res. Briefs*, 1989

8. Publications

Moin, P., "A new approach for large eddy simulation of turbulence and scalar transport," in *New Approaches and Concepts in Turbulence*, edited by Th. Dracos and A. Tsinober, 331-339, Birkhauser Verlag

Moin, P., Carati, D., Lund, T., Ghosal, S. & Akselvoll, K., "Developments and applications of dynamic models for large eddy simulation of complex flows" AGARD-CP-551, 1994

Moin, P. & Jimenez, J., "Large eddy simulation of complex turbulent flows," *AIAA-99-3099*, 1993

Neves, J., Moin, P. & Moser, R., "Effects of convex transverse curvature on wall-bounded turbulence, Part 1. The velocity and vorticity," *Journal of Fluid Mechanics*, vol. 272, 1994

Neves, J. & Moin, P., "Effects of convex transverse curvature on wall-bounded turbulence, Part 2. The pressure fluctuations," *Journal of Fluid Mechanics*, vol. 272, 1994

EXPLANATION OF FIGURES

Figure 1 Comparison of frequency spectrum of wall-pressure fluctuations with the experimental data (ZPG). (a) Outer variable scaling. Note that the data from simulation and the experiments appear to collapse at low frequencies. (b) Inner variable scaling. Note that the data from simulation and the experiments appear to collapse at high frequencies.

Figure 2 Convection velocity $U_c(r_x)$ as a function of streamwise spatial separation (ZPG). The large-scale structures corresponding to large separations in space have a convection velocity of about $0.8 U_o$ and small-scale motions have a smaller velocity, $0.7 U_o$.

Figure 3 Comparison of computed coefficient and skin friction coefficient with the experimental data of Watmuff.

Figure 4 Comparison of turbulent intensities with the experimental data of Watmuff in the adverse pressure gradient region.

Figure 5 Frequency spectrum of wall-pressure fluctuations (FPG + APG), outer variable scaling. Note that the results collapse at low frequencies. $x=0.5$ is in the favorable pressure gradient region and the remaining points are in the adverse pressure gradient regions.

Figure 6 Frequency spectrum of wall-pressure fluctuations (FPG + APG), inner variable scaling. The results collapse at high frequencies. Note that outer variable scaling with pressure scaled with p^2_{rms} is used. $x=0.5$ is in the favorable pressure gradient region and the remaining points are in the adverse pressure gradient regions.

Figure 7 Contour plot of two-point correlation of wall-pressure fluctuations as a function of streamwise and spanwise spatial separations (FPG + APG). Note that the contours are more elongated in the spanwise direction in the adverse pressure gradient region.

Figure 8 Convection velocity $U_c(r_x)$ as a function of streamwise spatial separation (FPG + APG). Note that the convection velocities are lower in the adverse pressure gradient case.

Figure 9 Streamlines, instantaneous spanwise vorticities and wall-shear stress distribution in the separated turbulent boundary layer. Note that the streaky structures disappear in the separated zone and reappear in the reattachment region.

Figure 10 Root-mean square pressure fluctuations as a function of the distance normal to the wall at several streamwise locations in the separated turbulent boundary layer.

Figure 11 Contours of instantaneous wall-pressure fluctuations in the (x,z) -planes. (a) $y = 0$. (b) $y = 13$.

Figure 12 Contour plot of two-point correlation of wall-pressure fluctuations as a function of streamwise and spanwise spatial separations (Separated flow).

Figure 13 Contour plot of two-point correlation of wall-pressure fluctuations as a function of streamwise spatial and temporal separations (Separated flow). The convection velocities are lower in both of the attachment and reattachment regions. Note that the characteristic length scale of the pressure fluctuations is increased after the attachment.

Figure 14 Frequency spectrum of wall-pressure fluctuations upstream of incipient detachment, outer variable scaling. (a) Normalized by local dynamic pressure. (b) Normalized by maximum Reynolds shear stress.

Figure 15 Frequency spectrum of wall-pressure fluctuations downstream of incipient detachment, outer variable scaling. (a) Normalized by local dynamic pressure. (b) Normalized by maximum Reynolds shear stress.

Figure 16 Streamwise distribution of wall-pressure fluctuations. (a) Normalized by inlet dynamic pressure. (b) Normalized by maximum Reynolds shear stress.

Comparison of frequency spectrum of wall-pressure fluctuations with experimental data (ZPG)

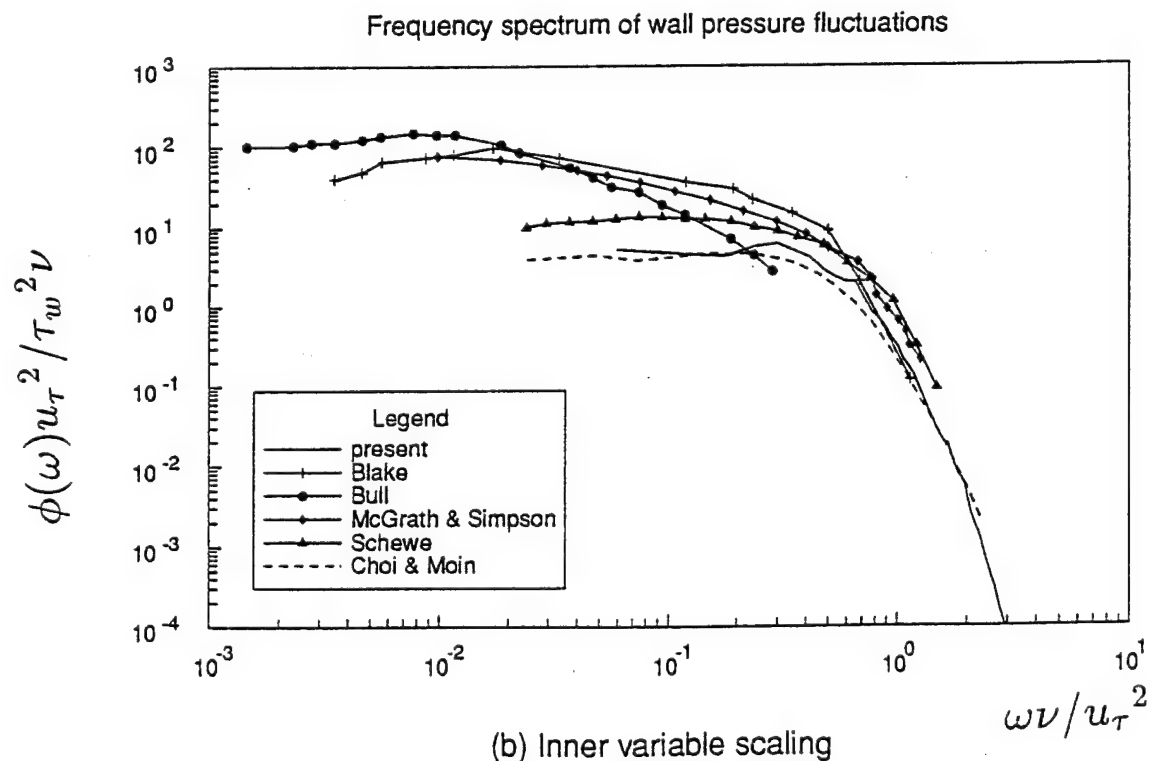
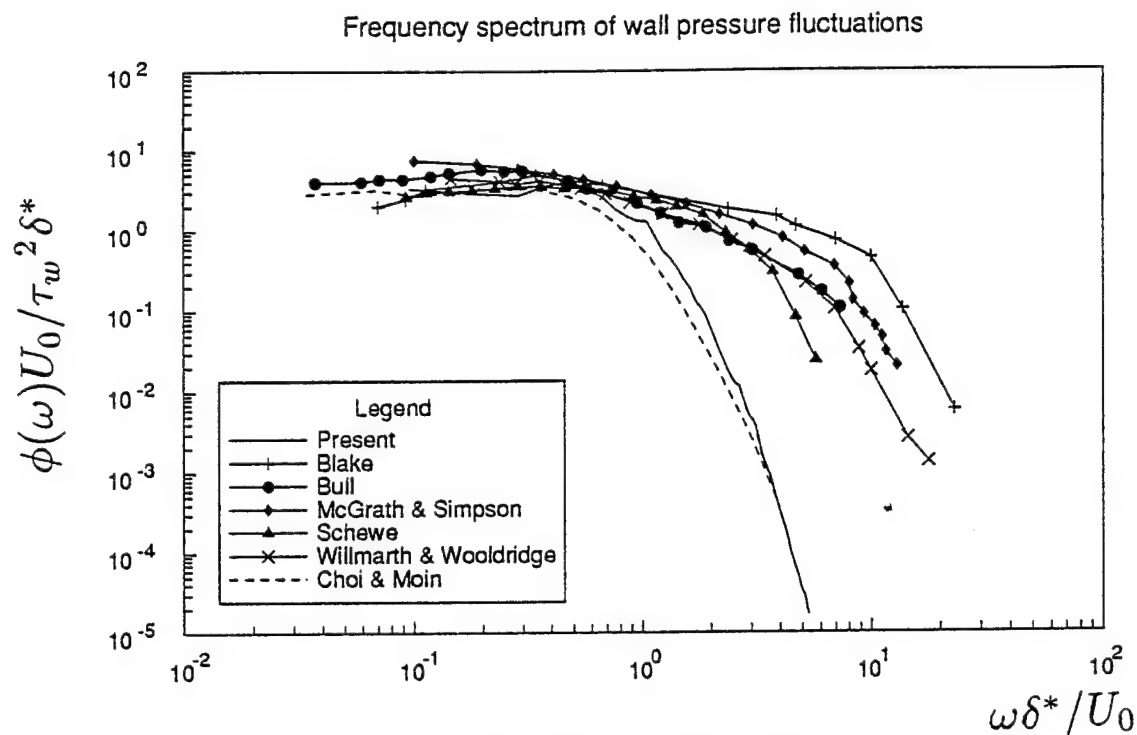


Figure 1 Comparison of frequency spectrum of wall-pressure fluctuations with the experimental data (ZPG). (a) Outer variable scaling. (b) Inner variable scaling.

Convection velocity U_c as a function of streamwise spatial separation (ZPG)

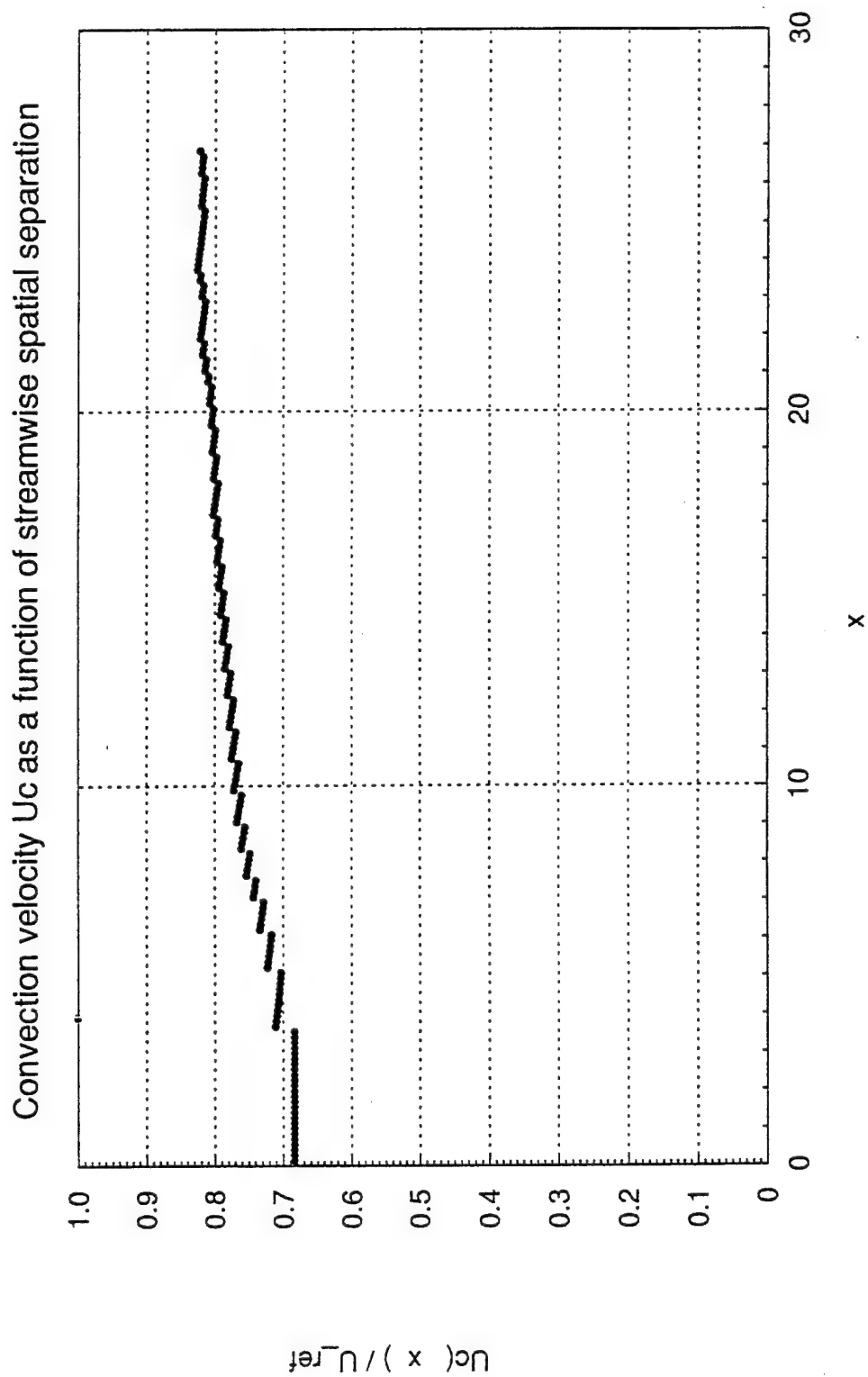


Figure 2 Convection velocity $U_c(r_x)$ as a function of streamwise spatial separation (ZPG).

Pressure coefficient C_p and skin friction coefficient C_f

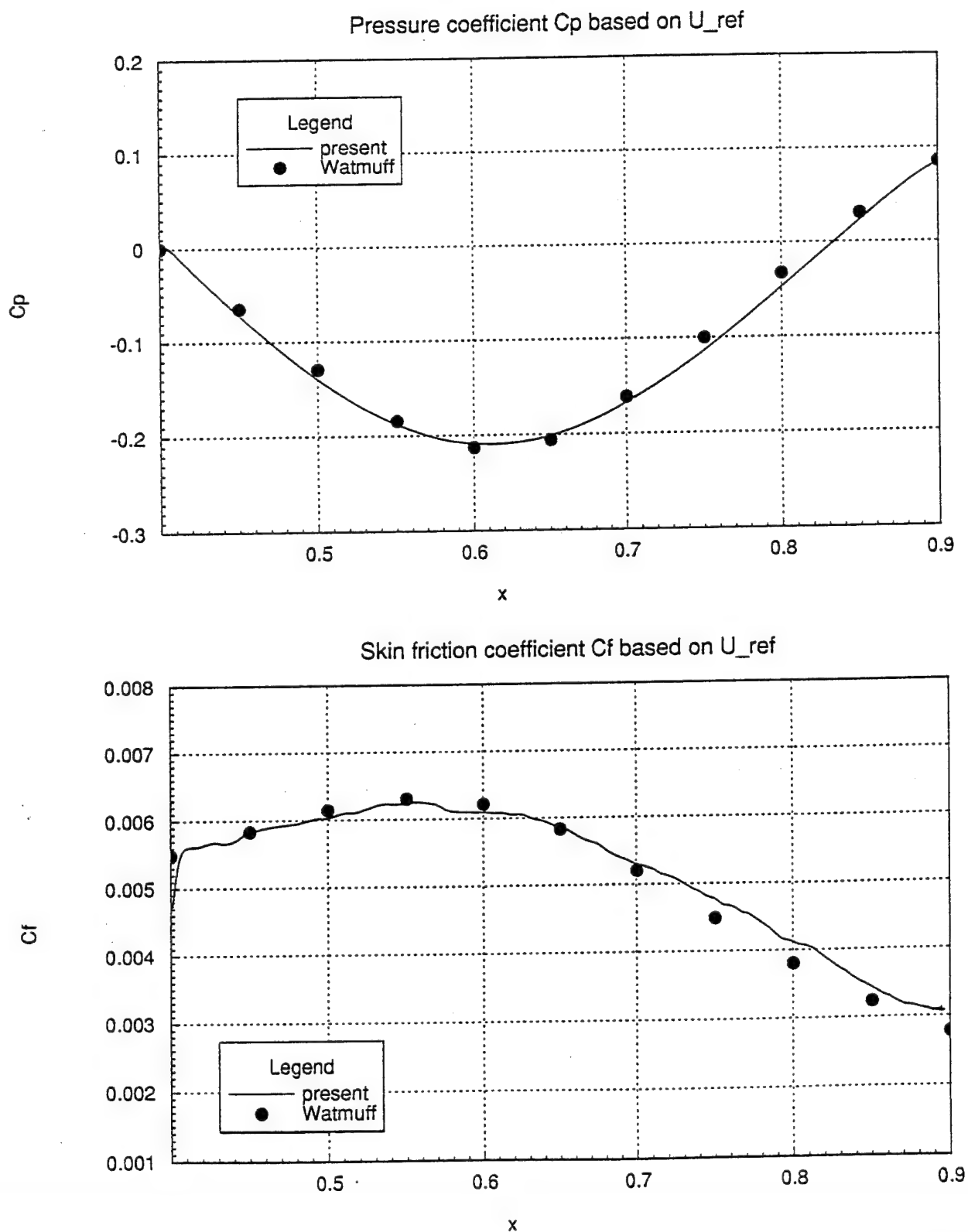


Figure 3 Comparison of computed coefficient and skin friction coefficient with the experimental data of Watmuff.

Turbulence intensities in the APG region

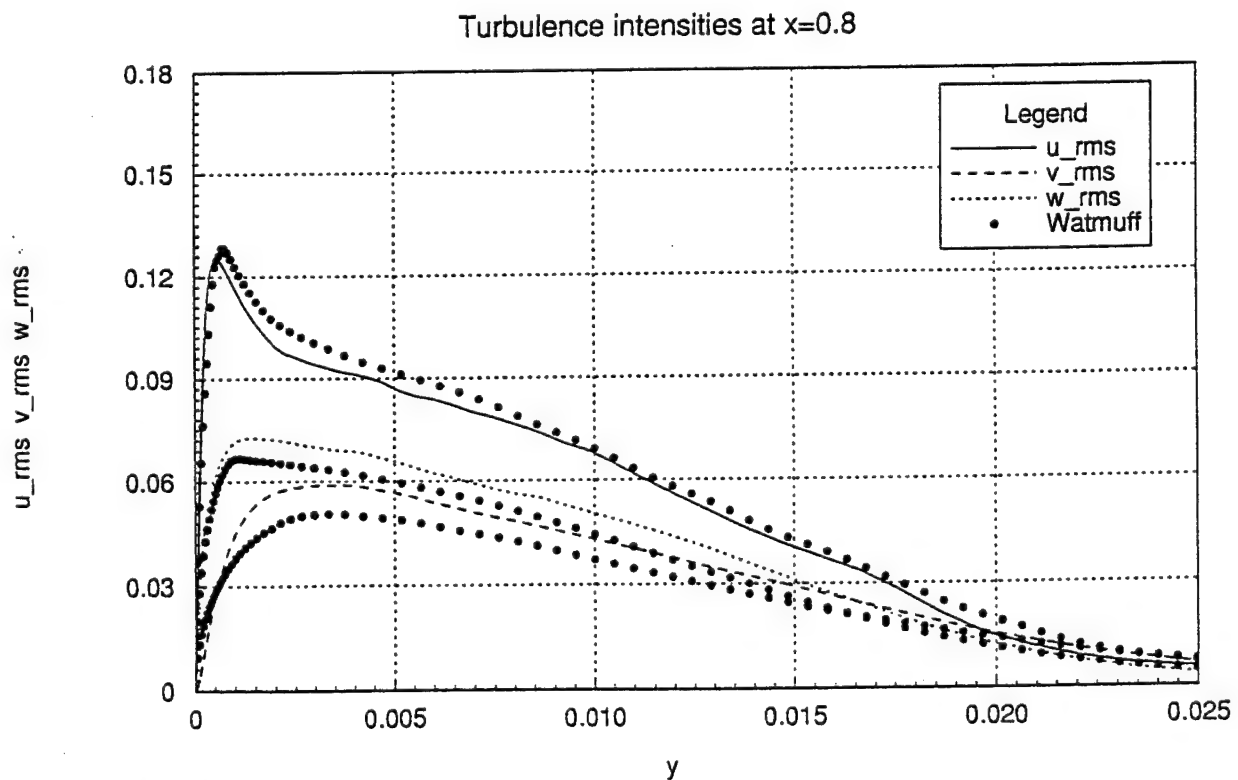
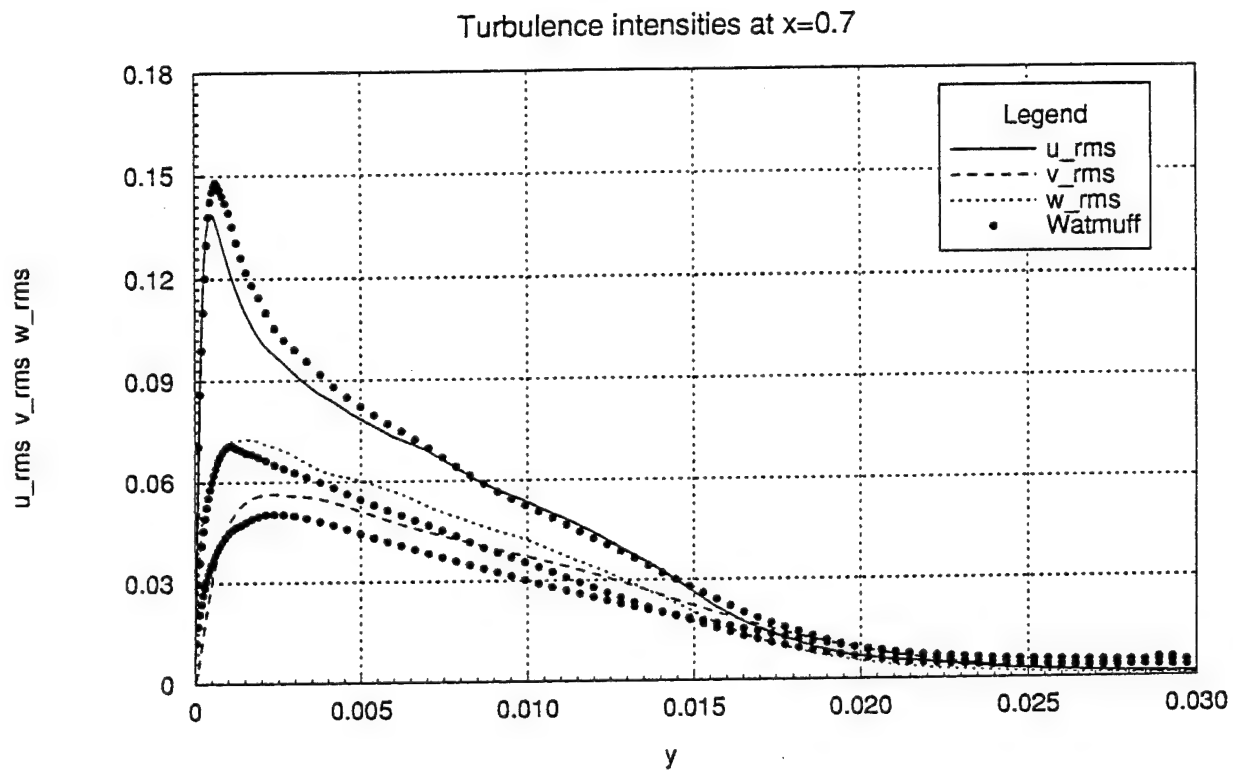


Figure 4 Comparison of turbulent intensities with the experimental data of Watmuff in the adverse pressure gradient region.

Frequency spectrum of wall-pressure fluctuations (FPG+APG flow)

Outer variable(U_∞) Scaling

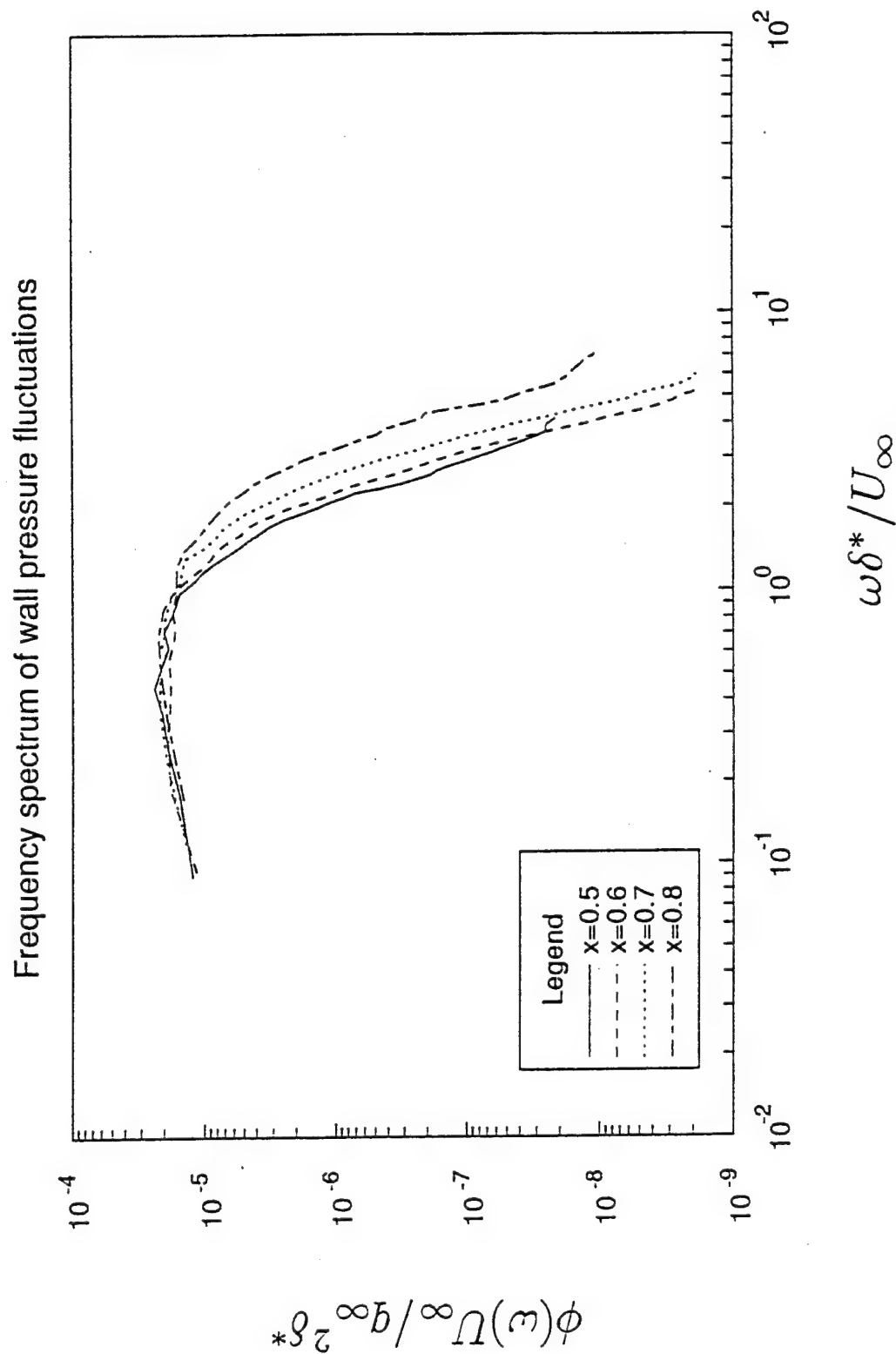


Figure 5 Frequency spectrum of wall-pressure fluctuations (FPG + APG), outer variable scaling. Note that the results collapse at low frequencies. $x=0.5$ is in the favorable pressure gradient region and the remaining points are in the adverse pressure gradient regions.

Frequency spectrum of wall-pressure fluctuations (FPG+APG flow)

p_{rms} Scaling

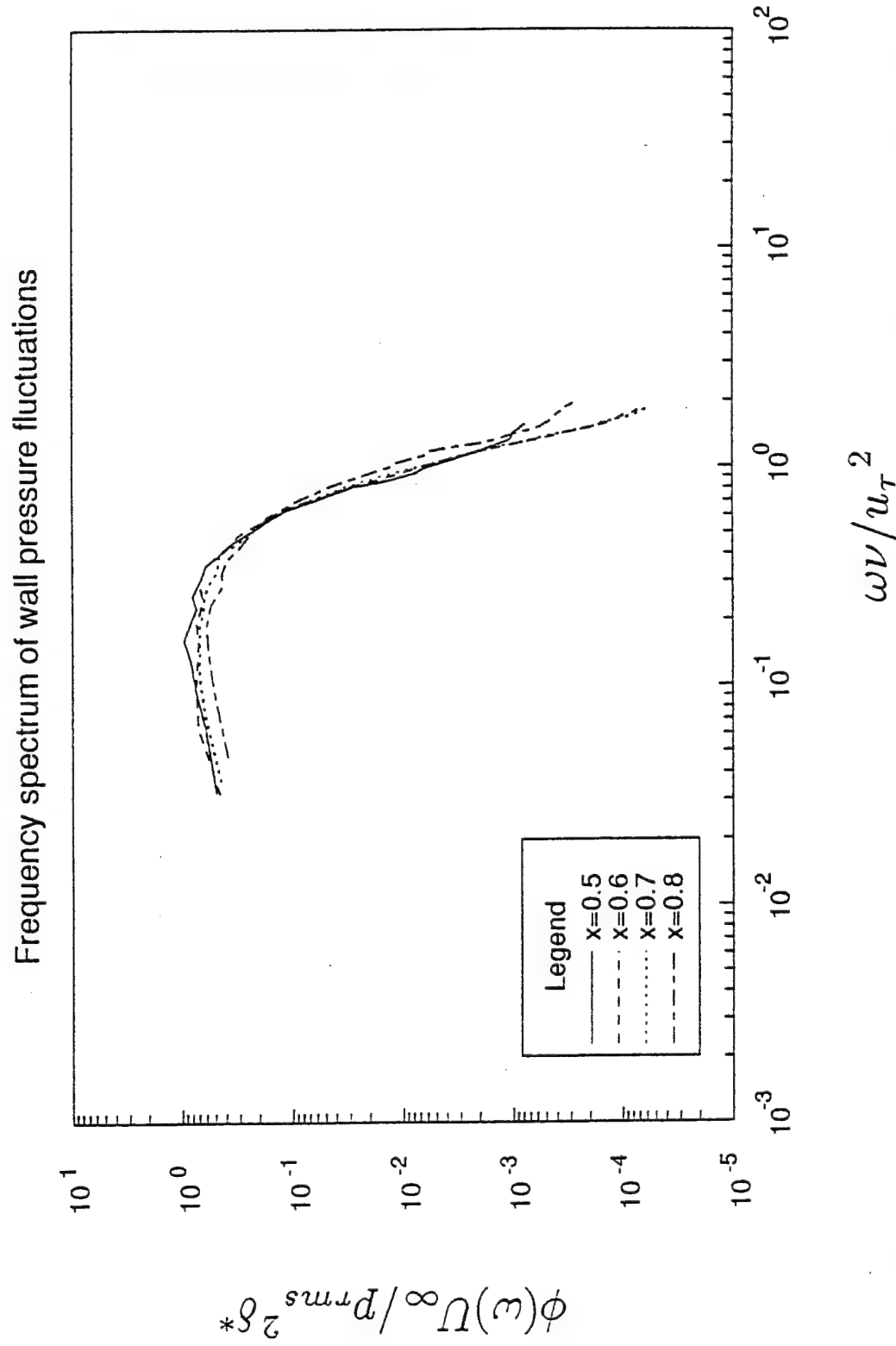
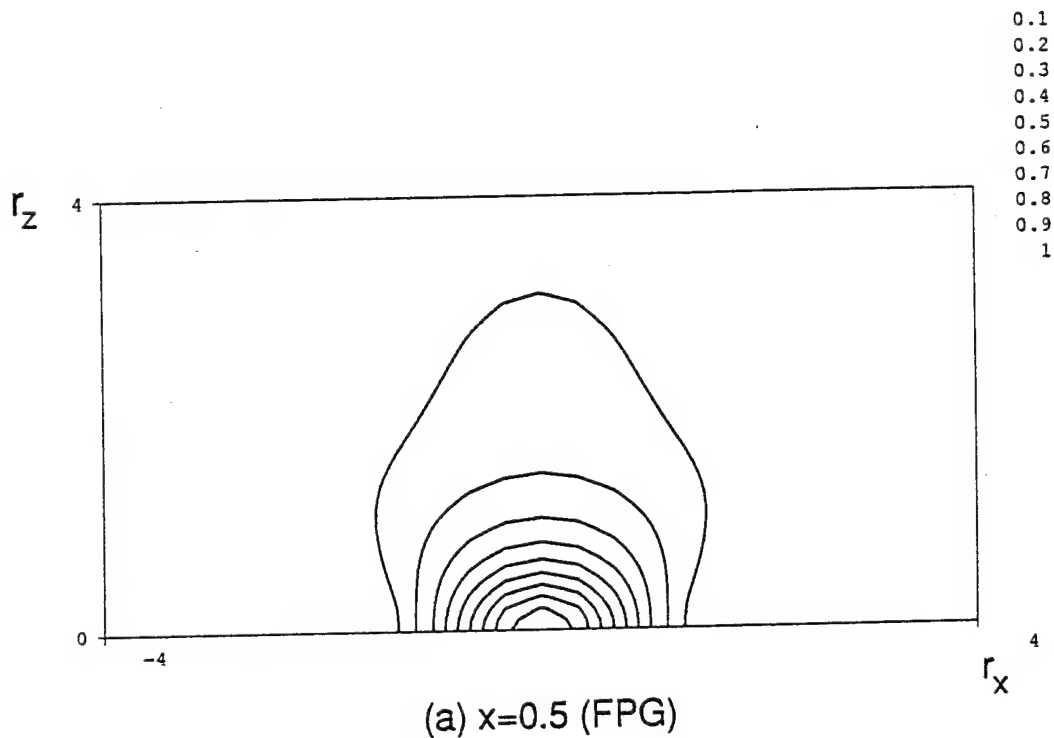


Figure 6 Frequency spectrum of wall-pressure fluctuations (FPG + APG). Note that the outer variable scaling with pressure scaled with p_{rms}^2 is used. $x=0.5$ is in the favorable pressure gradient region and the remaining points are in the adverse pressure gradient regions.

Contour plots of two-point correlation of wall-pressure fluctuations in the (x,z)-plane

Contour plot of two point correlation of p'



Contour plot of two point correlation of p'

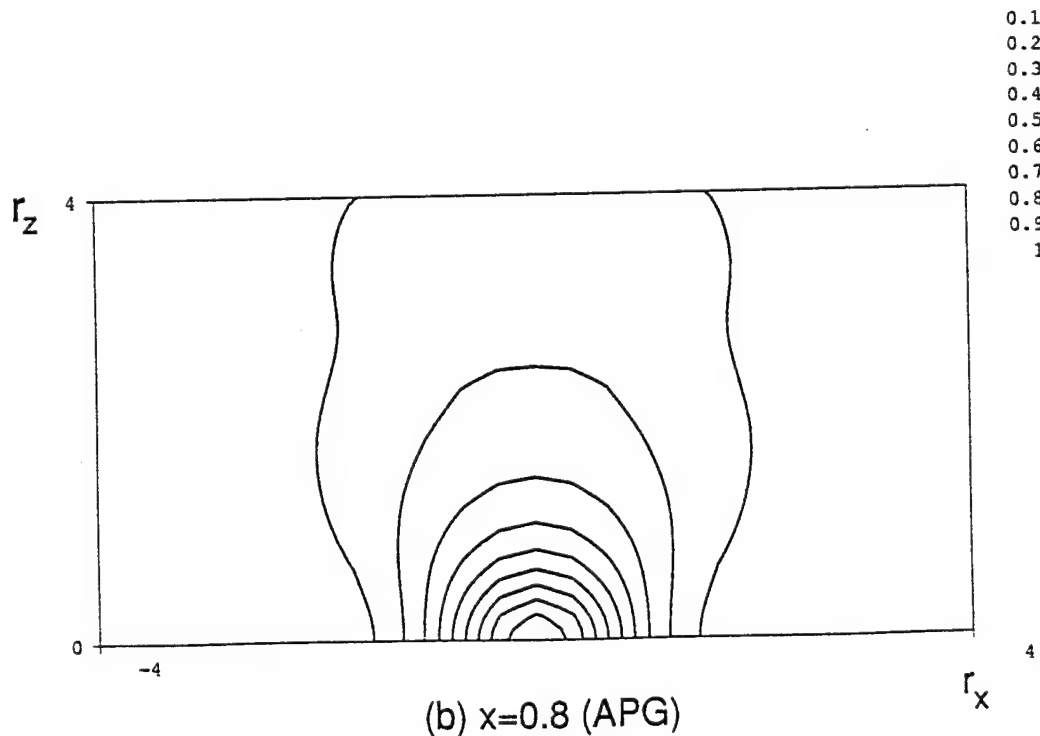


Figure 7 Contour plot of two-point correlation of wall-pressure fluctuations as a function of streamwise and spanwise spatial separations (FPG + APG). (a) $x=0.5$ (FPG region). (b) $x=0.8$ (APG region)

Convection velocity U_c as a function of streamwise spatial separation (FPG+APG)

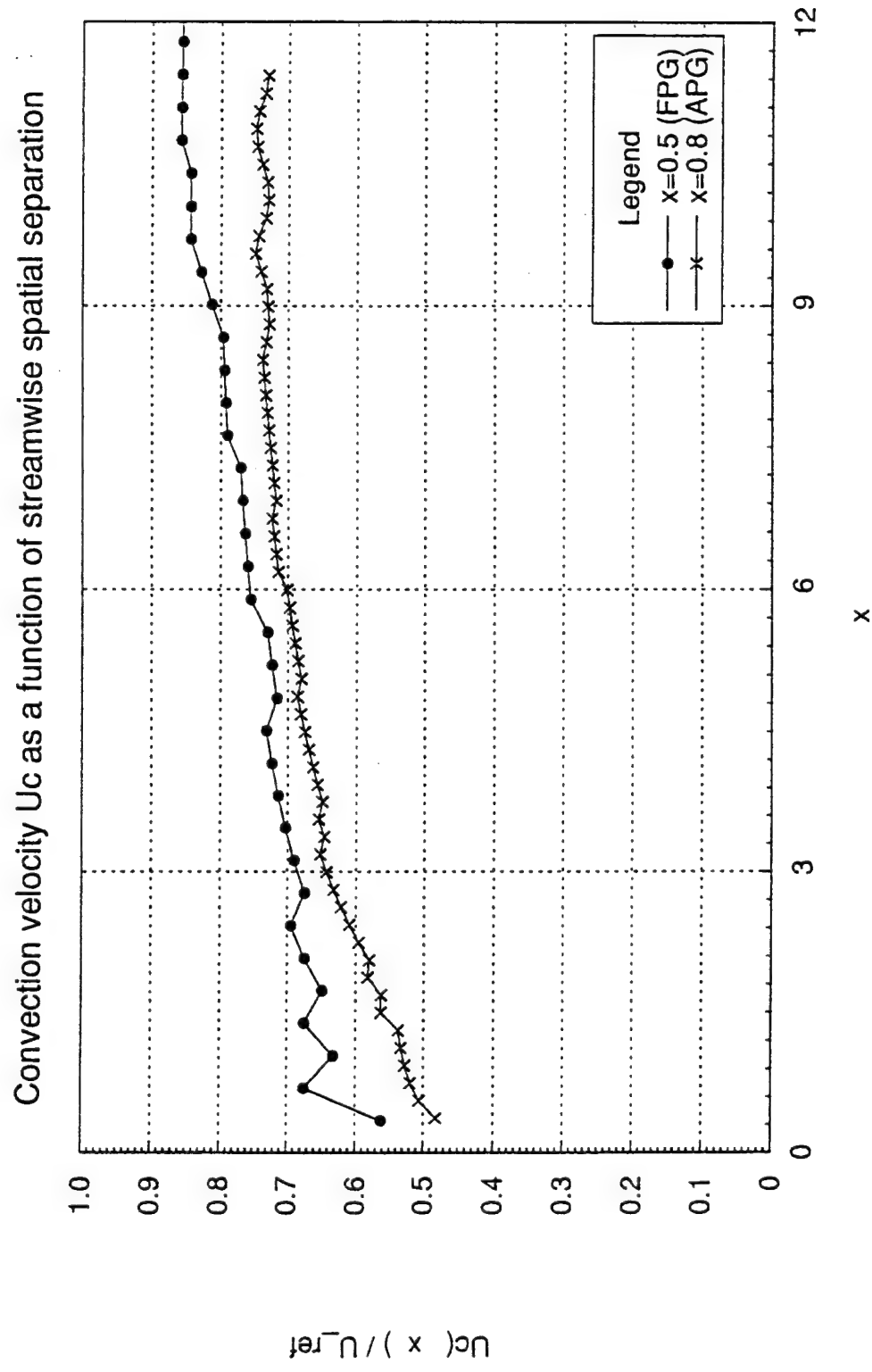


Figure 8 Convection velocity $U_c(r_x)$ as a function of streamwise spatial separation (FPG + APG). Note that the convection velocities are lower in the adverse pressure gradient case.

Characteristics of the separated turbulent boundary layer

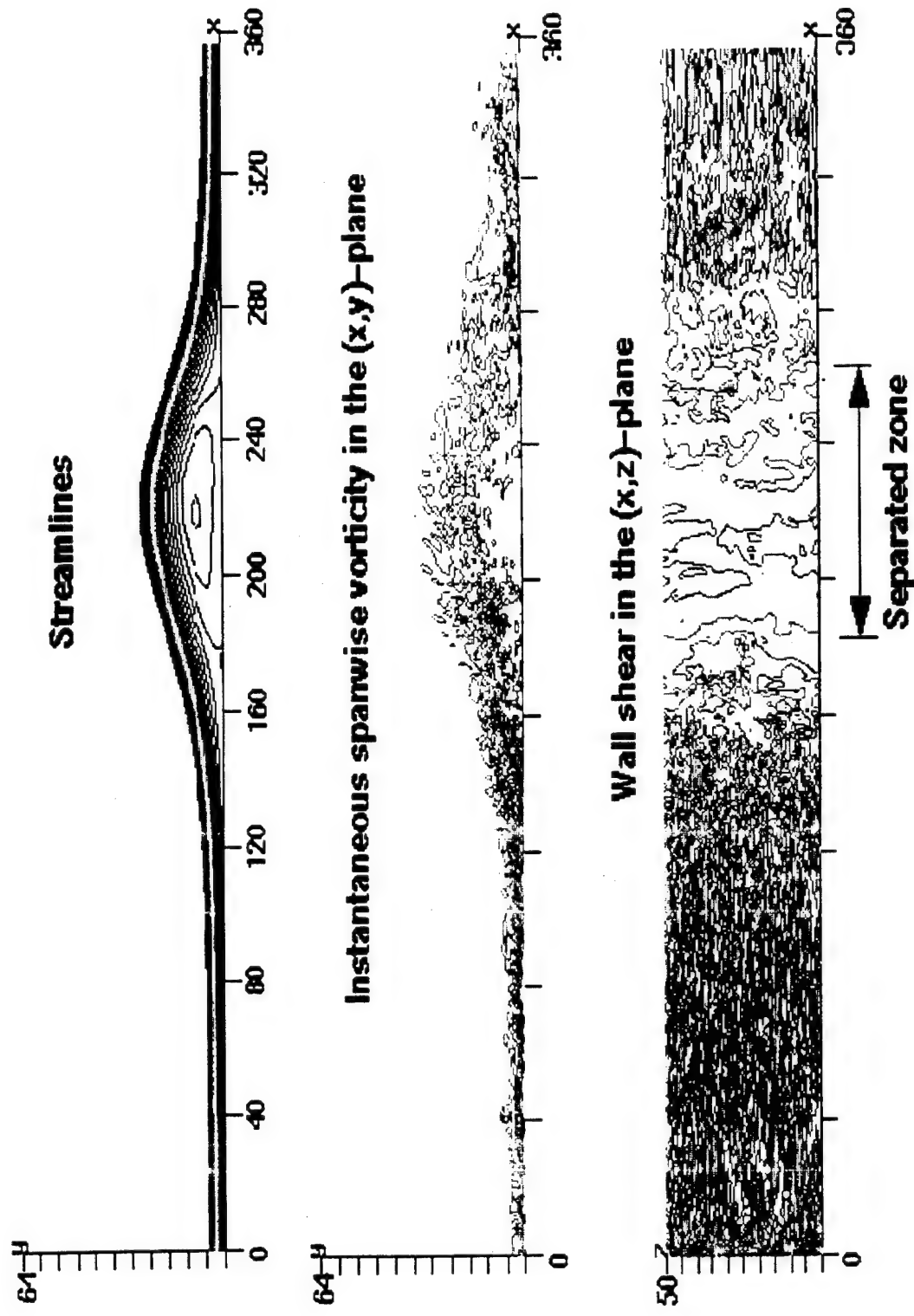


Figure 9 Streamlines, instantaneous spanwise vorticity and wall-shear stress

Root-mean square pressure fluctuations

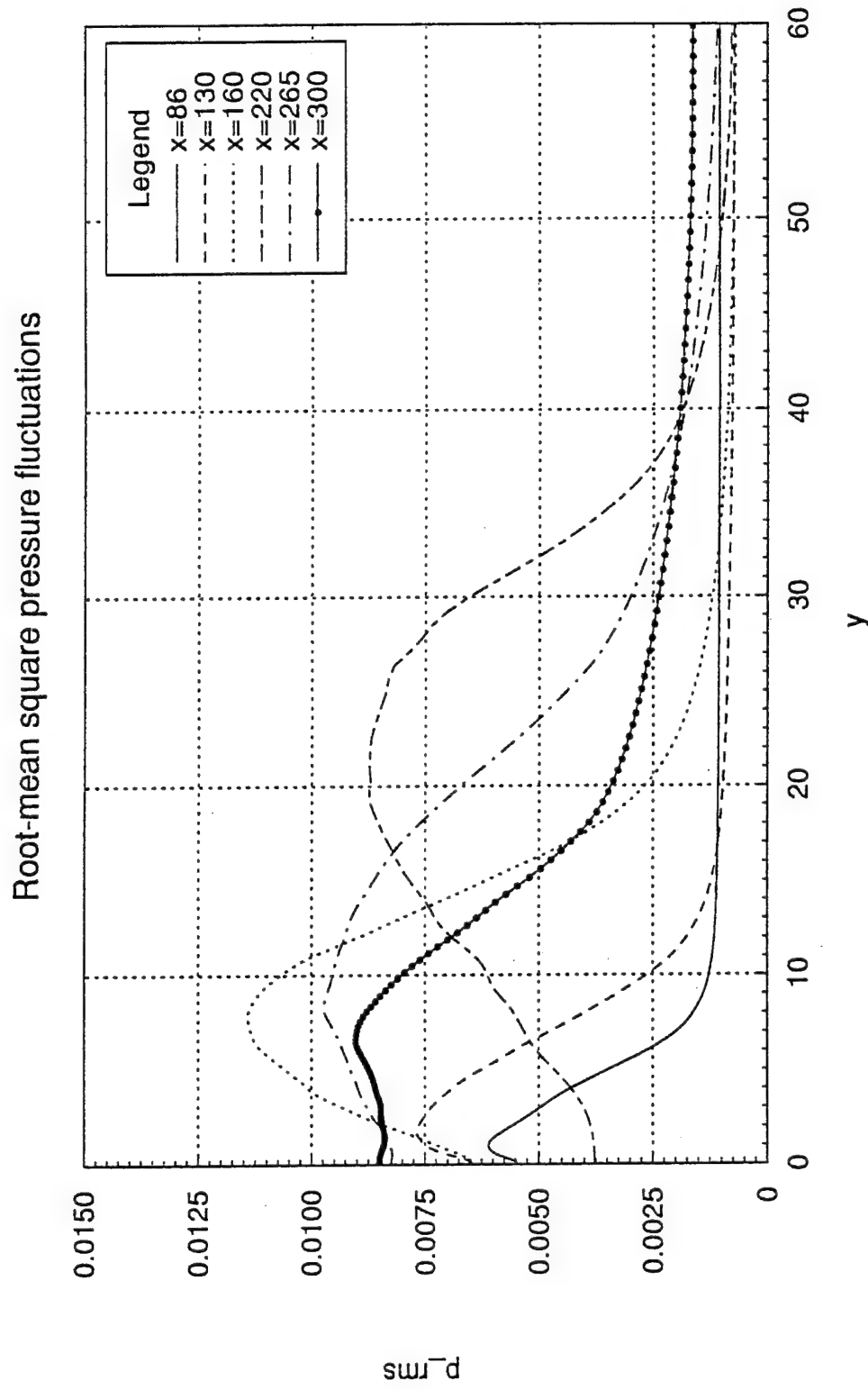
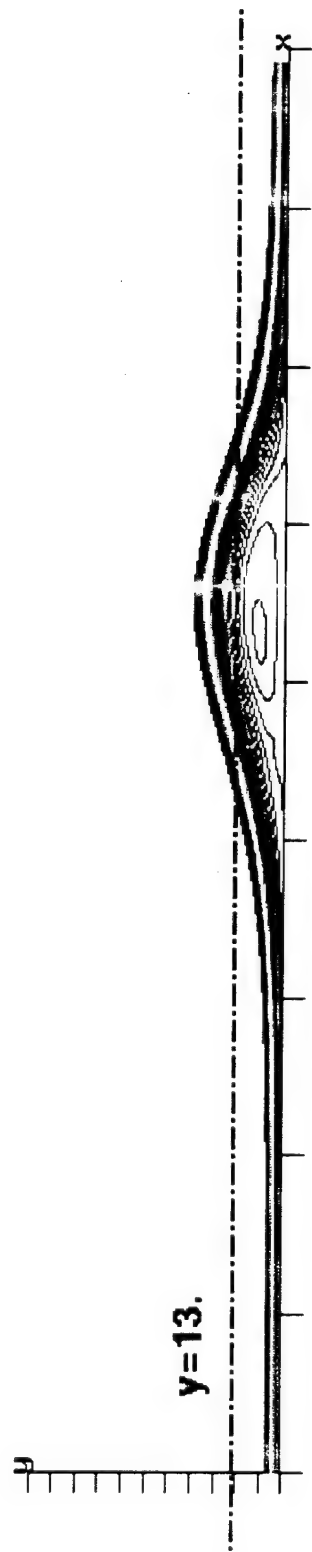


Figure 10 Root-mean square pressure fluctuations as a function of the distance normal to the wall at several streamwise locations in the separated turbulent boundary layer.



Contours of pressure fluctuations in the $(x-z)$ plane



(a) $y=0$.



(b) $y=13$

Figure 11 Contours of instantaneous wall-pressure fluctuations in the (x, z) -plane

Contour plot of two-point correlation of wall-pressure fluctuations as a function of spatial separations

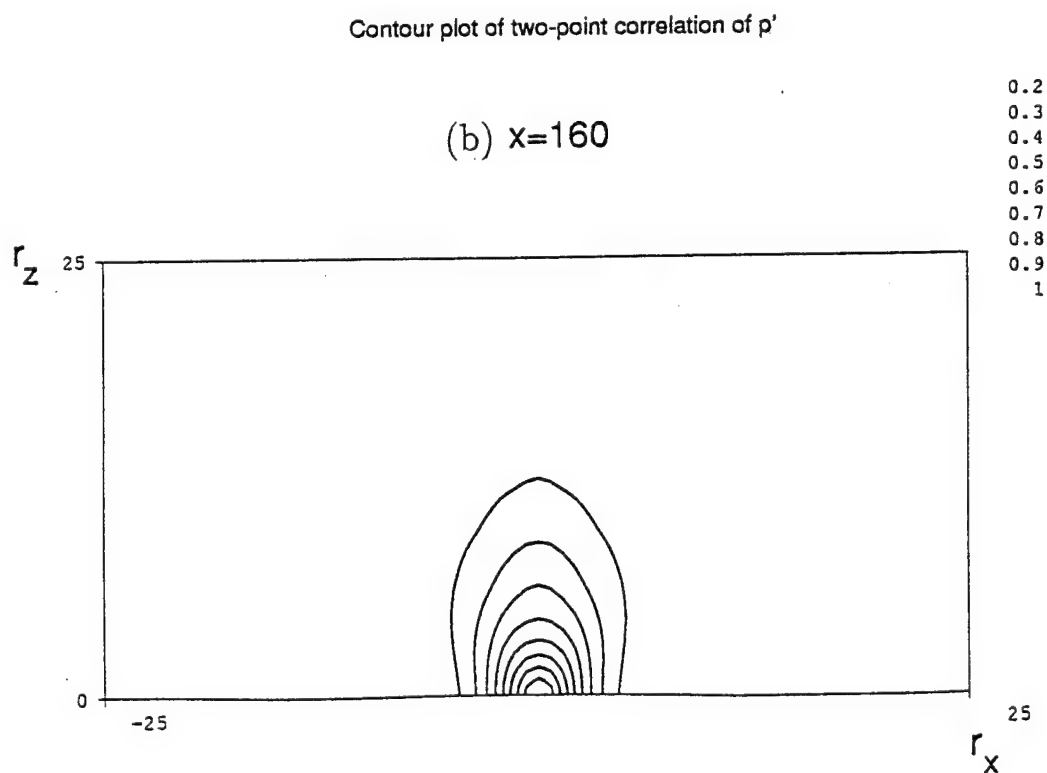
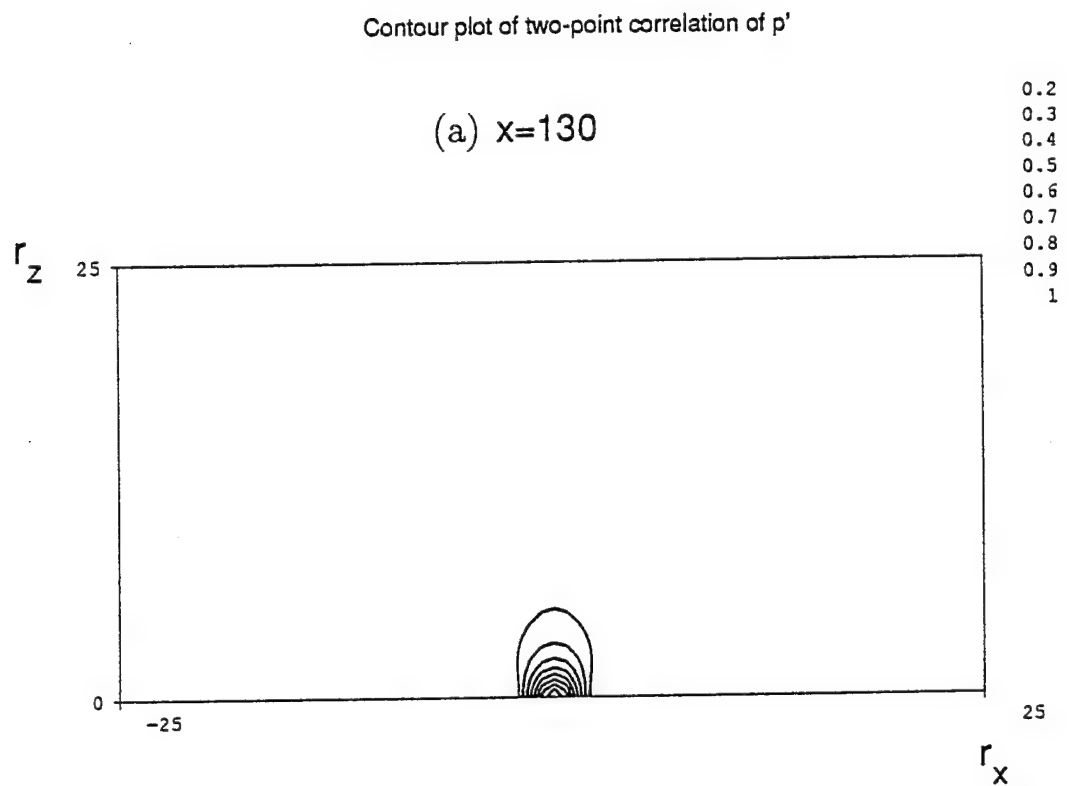


Figure 12 Contour plot of two-point correlation of wall-pressure fluctuations as a function of streamwise and spanwise spatial separations (Separated flow). (a) $x=130$. (b) $x=160$. (c) $x=220$. (d) $x=300$.

Contour plot of two-point correlation of wall-pressure fluctuations as a function of spatial separations

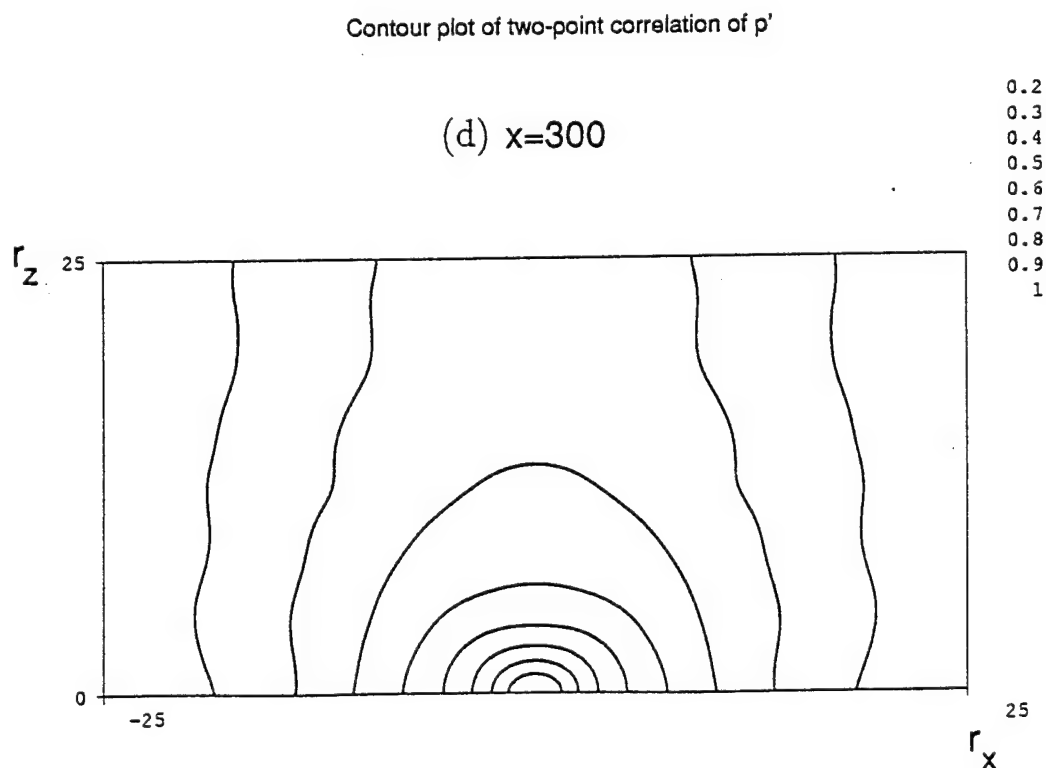
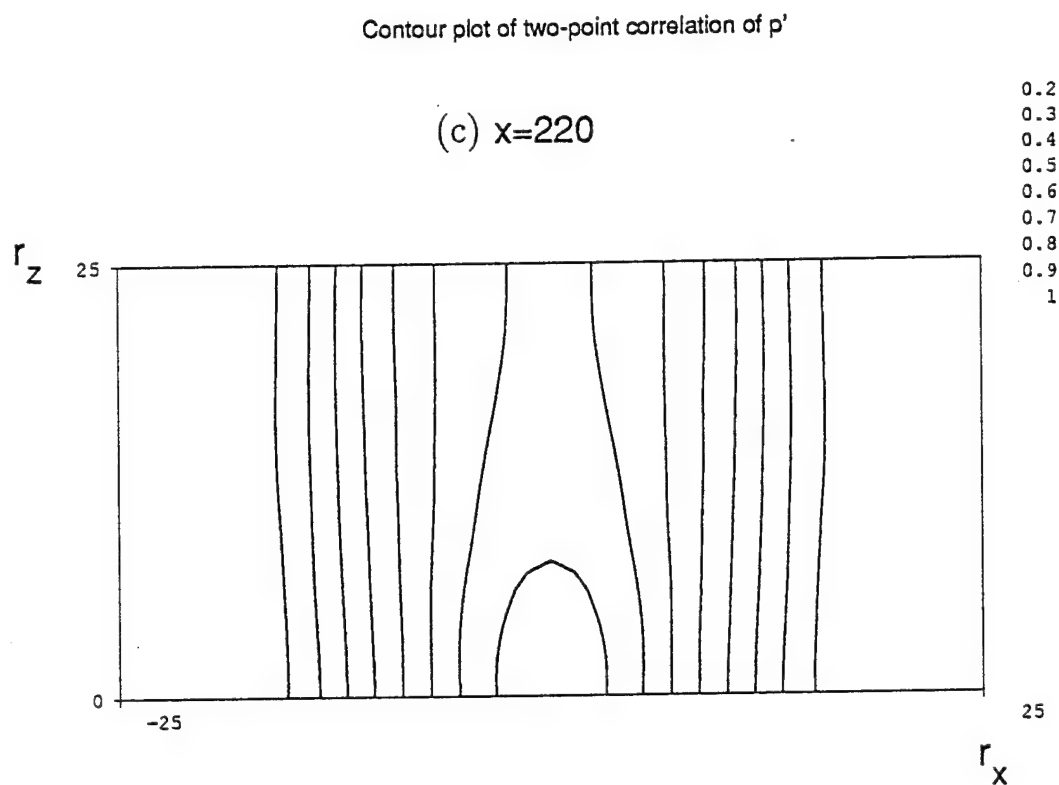


Figure 12 Contour plot of two-point correlation of wall-pressure fluctuations as a function of streamwise and spanwise spatial separations (Separated flow). (a) $x=130$. (b) $x=160$. (c) $x=220$. (d) $x=300$.

Contour plot of two-point correlation of wall-pressure fluctuations as a function of spatial and temporal separations

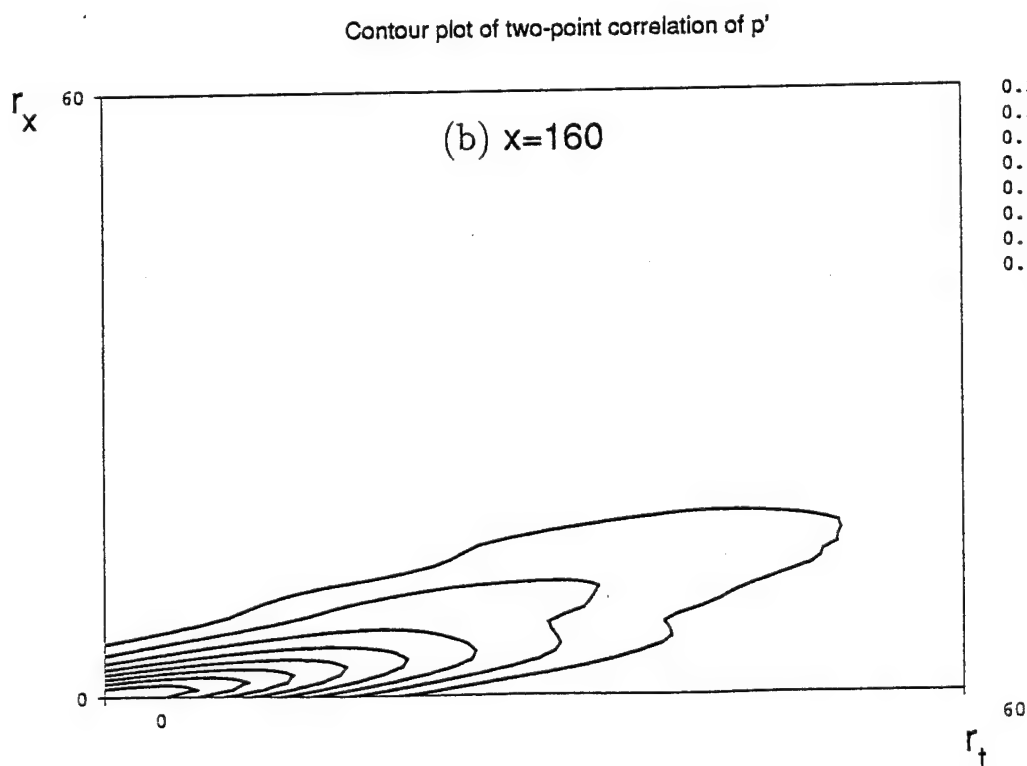
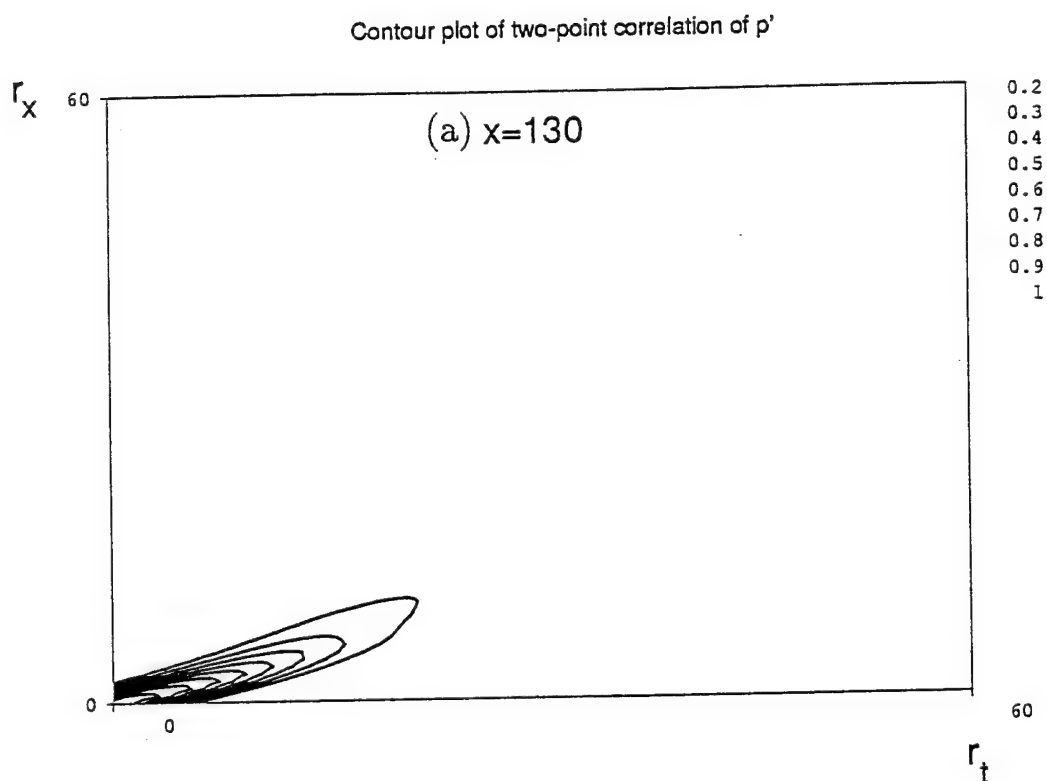


Figure 13 Contour plot of two-point correlation of wall-pressure fluctuations as a function of streamwise spatial and temporal separations (Separated flow). (a) $x=130$. (b) $x=160$. (c) $x=220$. (d) $x=300$.

Contour plot of two-point correlation of wall-pressure fluctuations as a function of spatial and temporal separations

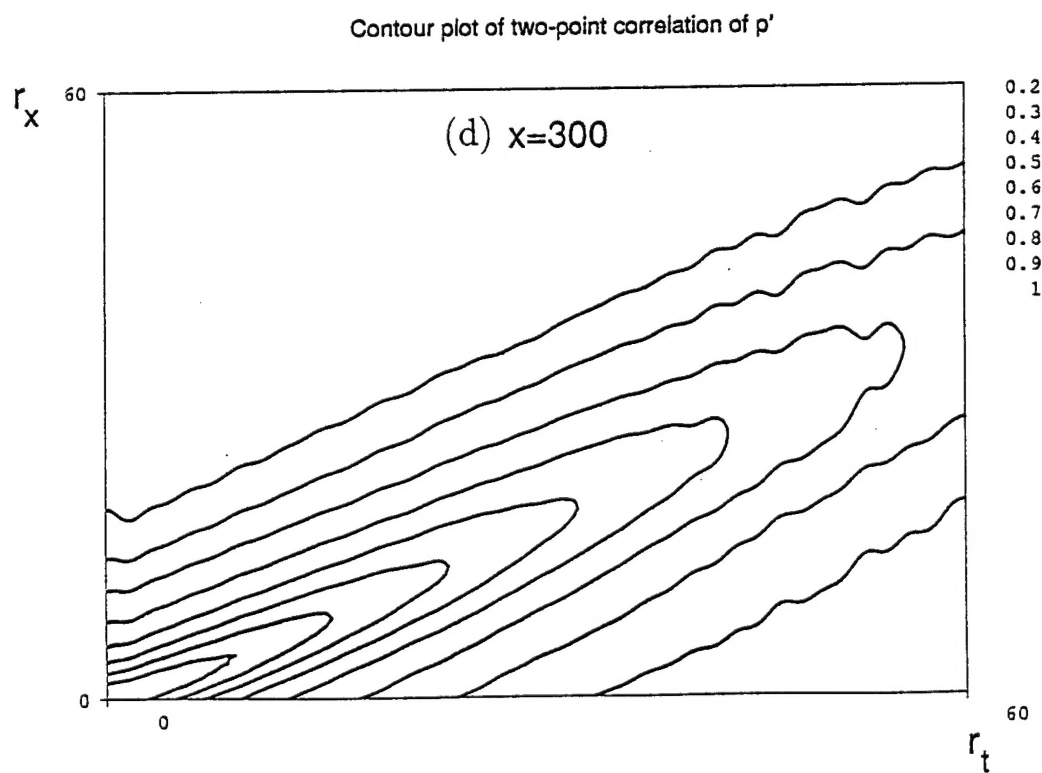
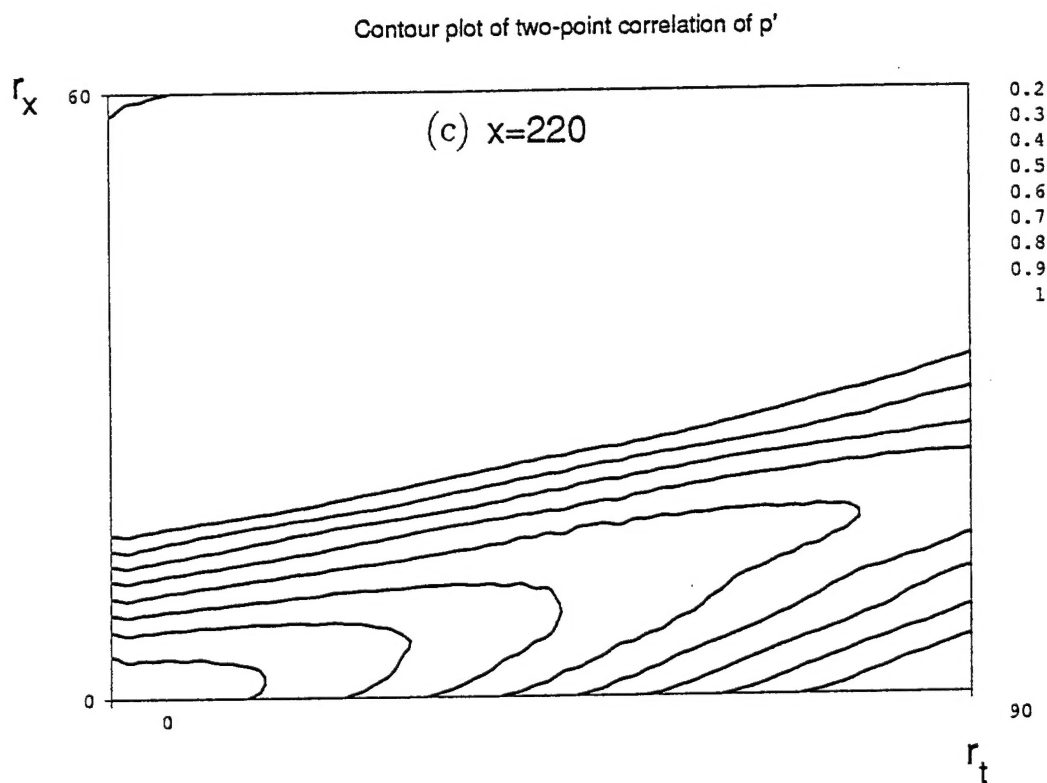


Figure 13 Contour plot of two-point correlation of wall-pressure fluctuations as a function of streamwise spatial and temporal separations (Separated flow). (a) $x=130$. (b) $x=160$. (c) $x=220$. (d) $x=300$.

Wall-pressure spectra upstream of incipient detachment

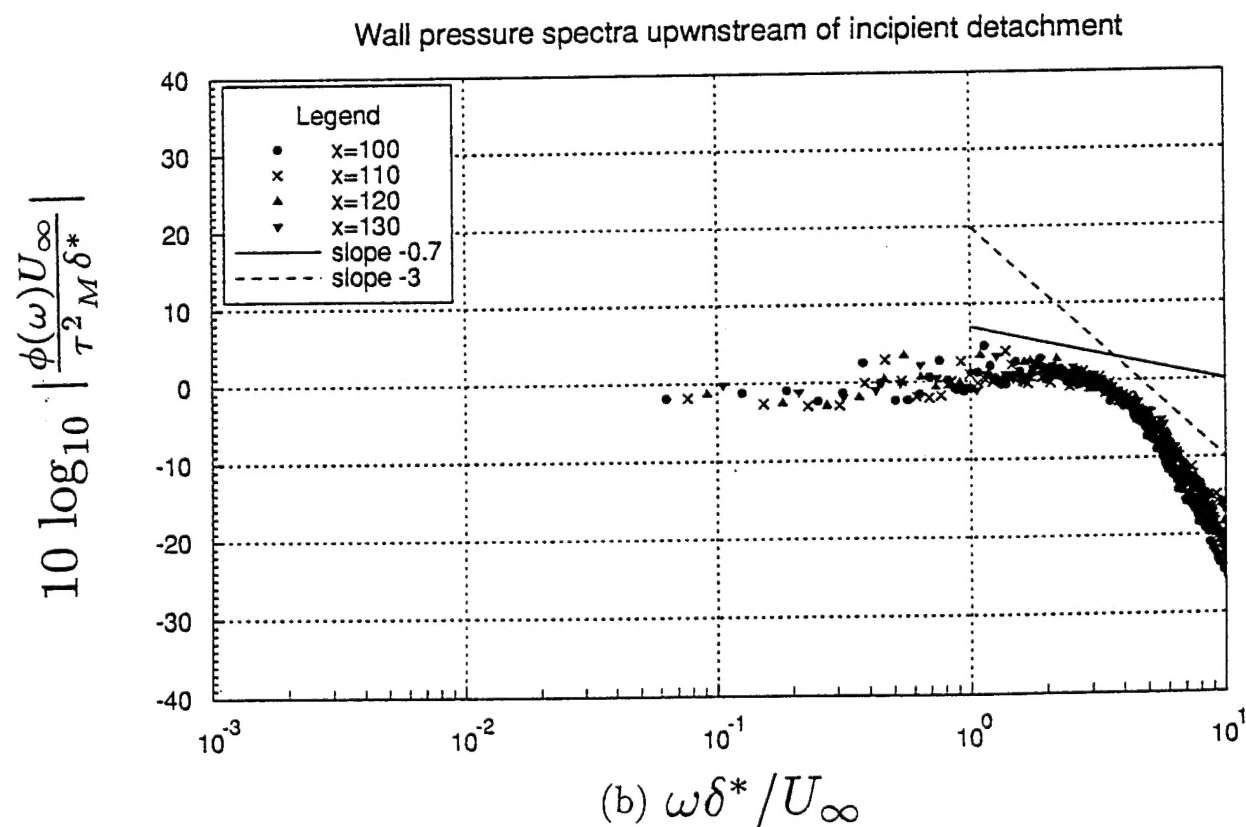
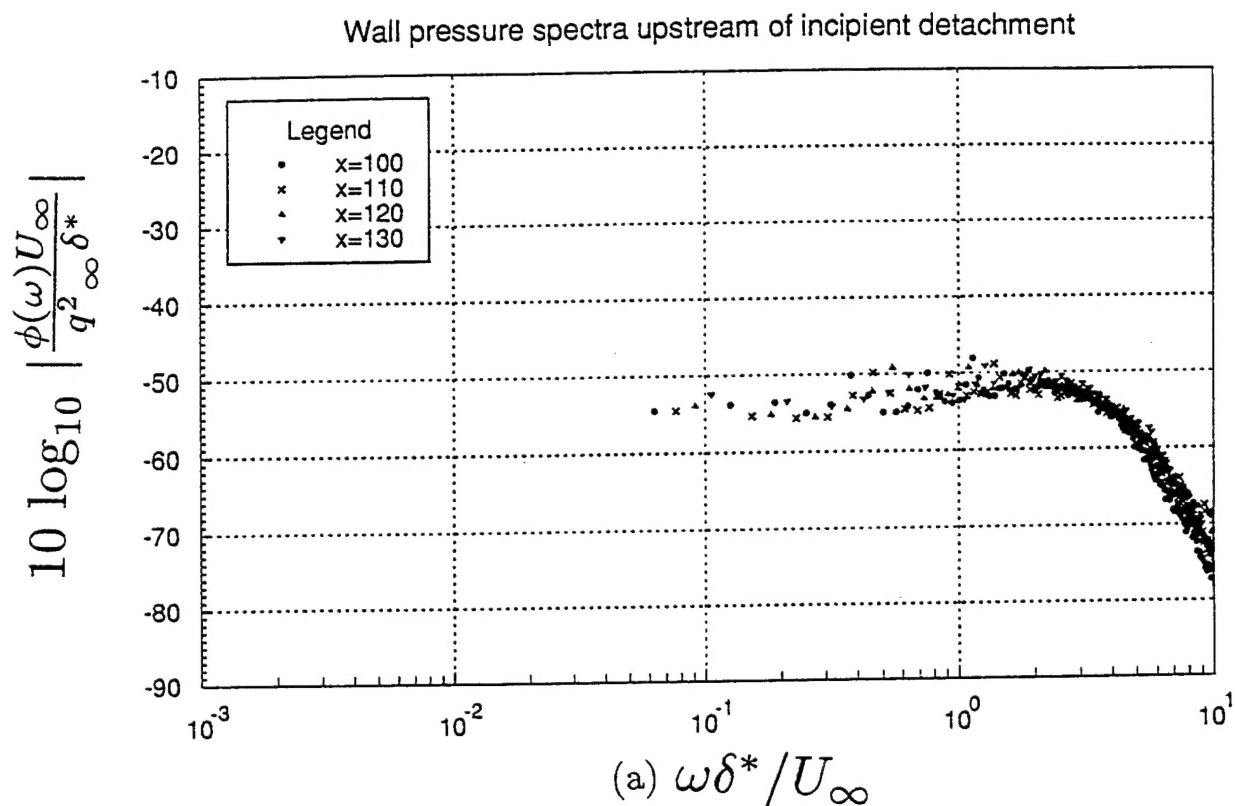


Figure 14 Frequency spectrum of wall-pressure fluctuations upstream of incipient detachment, outer variable scaling. (a) Normalized by local dynamic pressure. (b) Normalized by maximum Reynolds shear stress.

Wall-pressure spectra downstream of incipient detachment

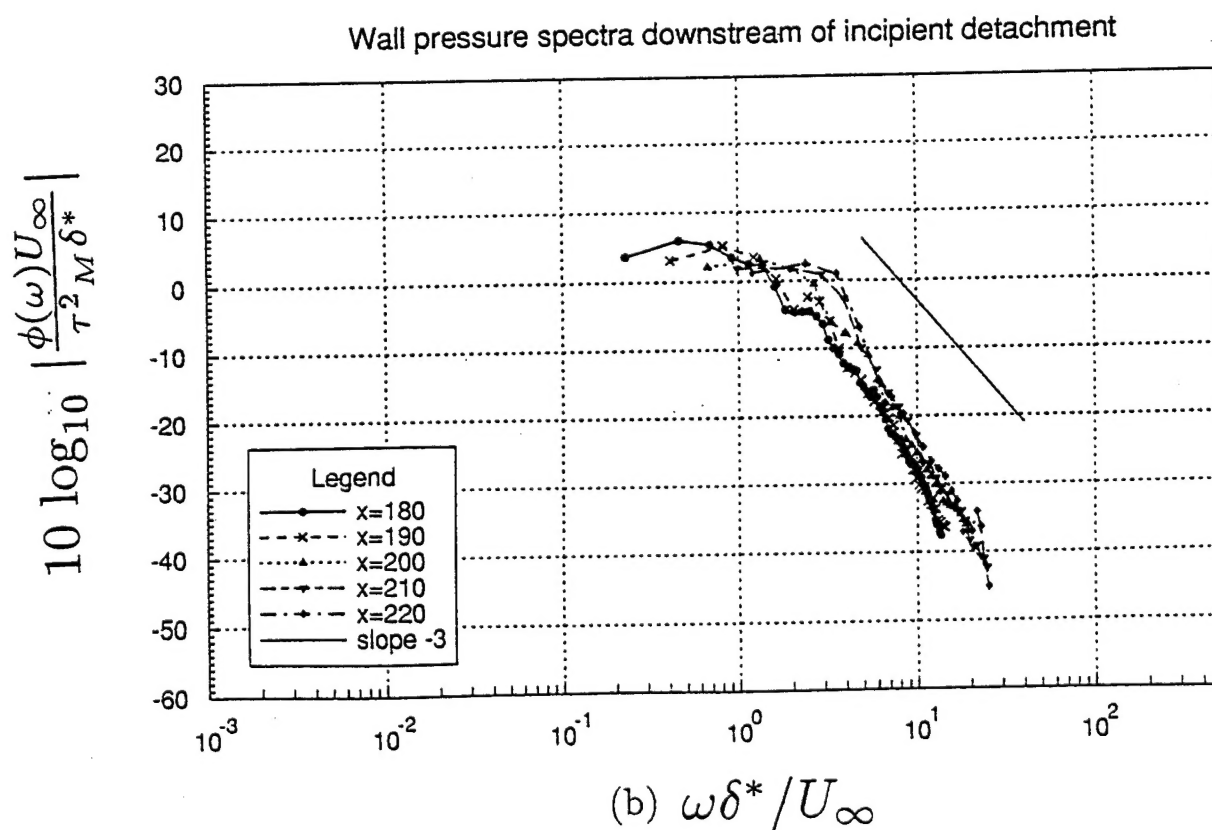
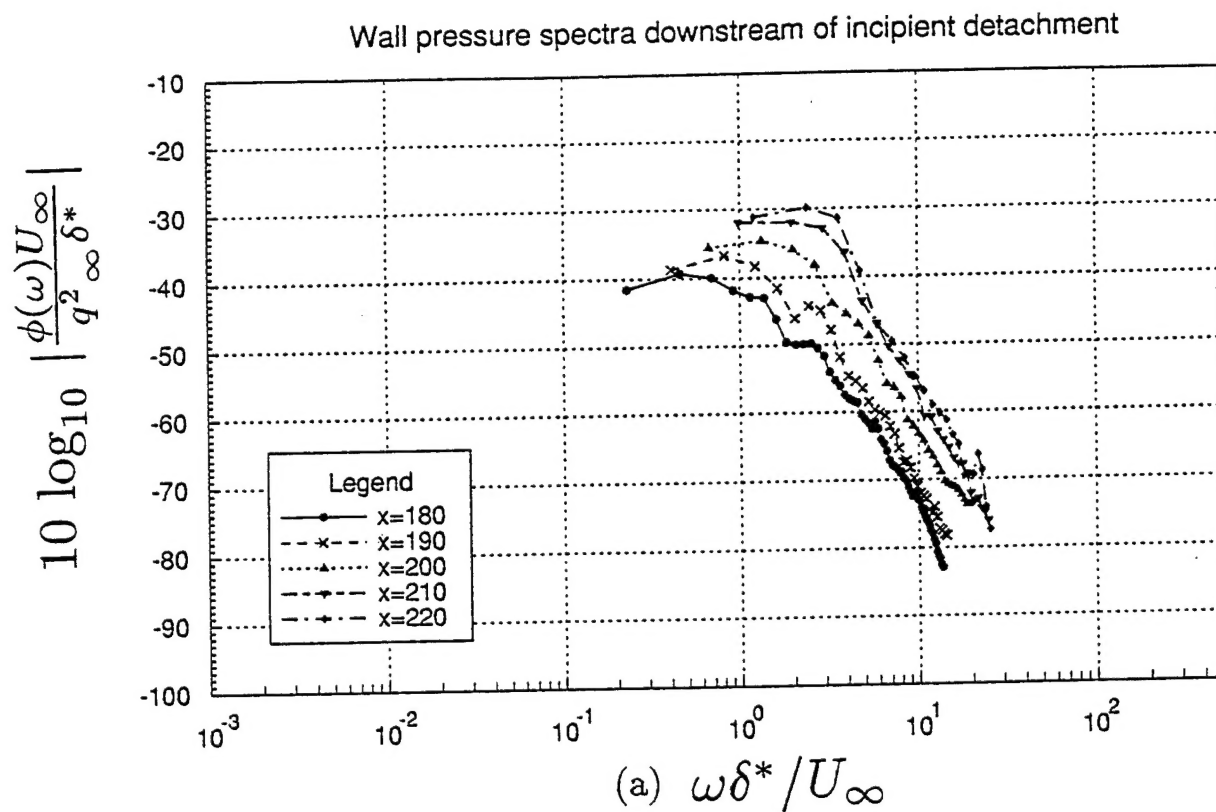


Figure 15 Frequency spectrum of wall-pressure fluctuations downstream of incipient detachment, outer variable scaling. (a) Normalized by local dynamic pressure. (b) Normalized by maximum Reynolds shear stress.

Streamwise distribution of wall-pressure fluctuations

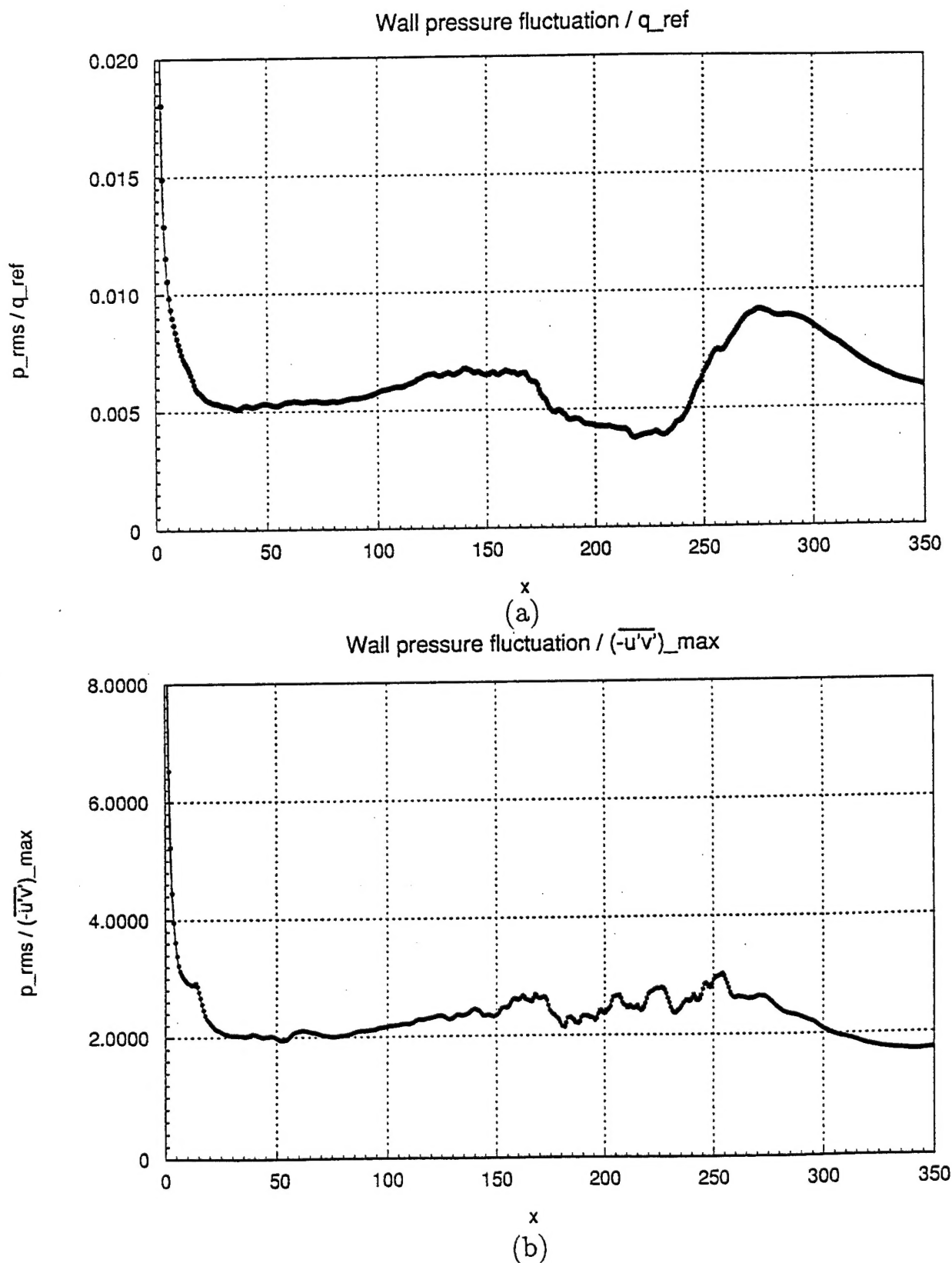


Figure 16 Streamwise distribution of wall-pressure fluctuations. (a) Normalized by inlet dynamic pressure. (b) Normalized by maximum Reynolds shear stress.